Supplementary Information

Table of Contents

Part A. Supplementary figures

Suppl. Fig. 1

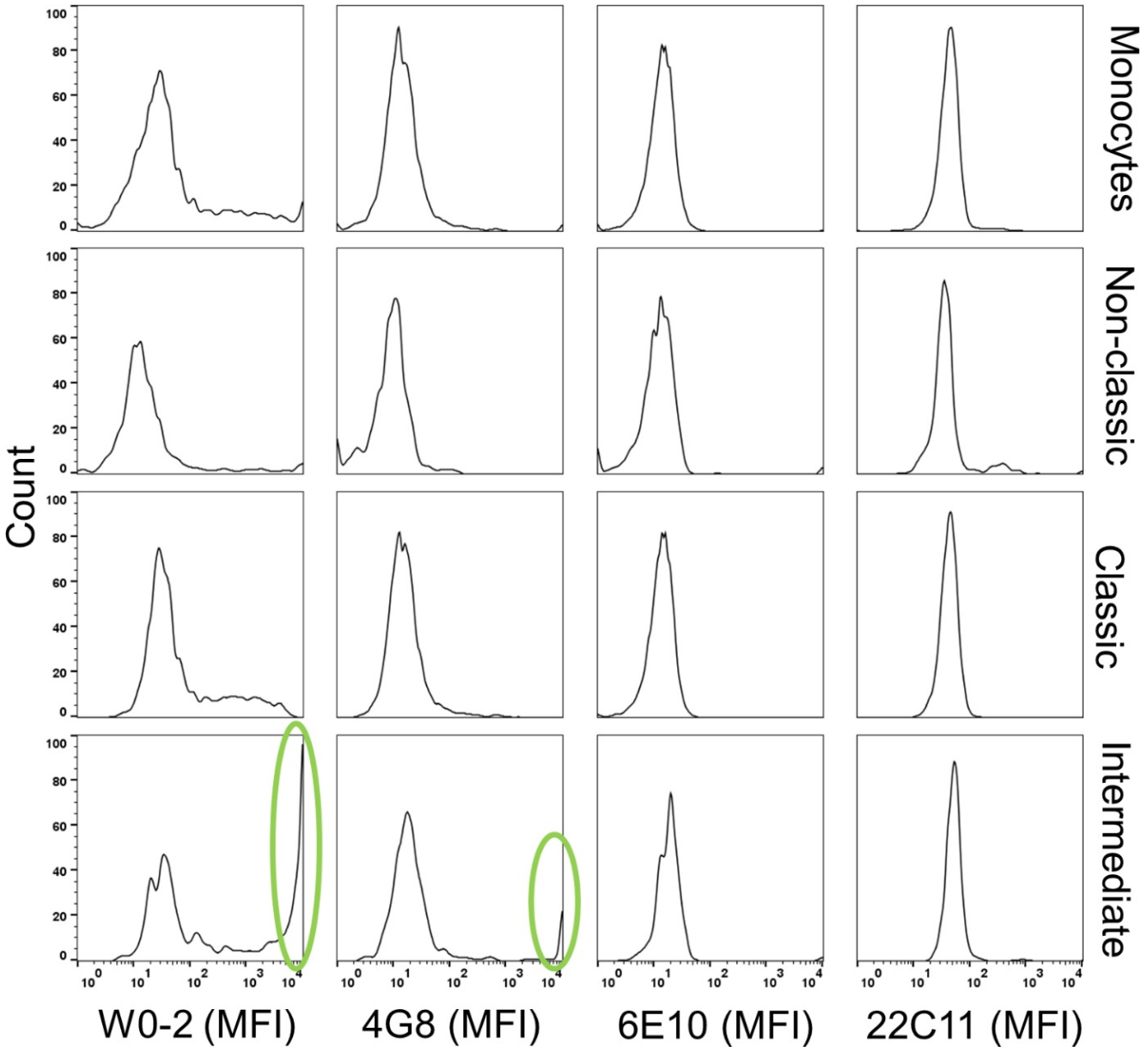

Suppl. Fig. 1: Comparative analysis of anti-Aβ monoclonal antibodies. Several anti-human Aβ monoclonal antibodies for their ability to identify Aβ-binding monocytes in the six blood samples (3 CU, 2 MCI, and 1 AD-Dementia) were assessed using flow cytometry. The antibodies included clones W0-2, 4G8, and 6E10, with 22C11, an anti-APP antibody, serving as a control. Results showed that most monocytes in the blood did not carry Aβ, with only a very small number showing Aβ binding. Among the antibodies tested, W0-2 demonstrated the highest sensitivity, followed by 4G8 and 6E10. In contrast, 22C11 was unable to recognize Aβ on the surface of monocytes.

Suppl. Fig. 2

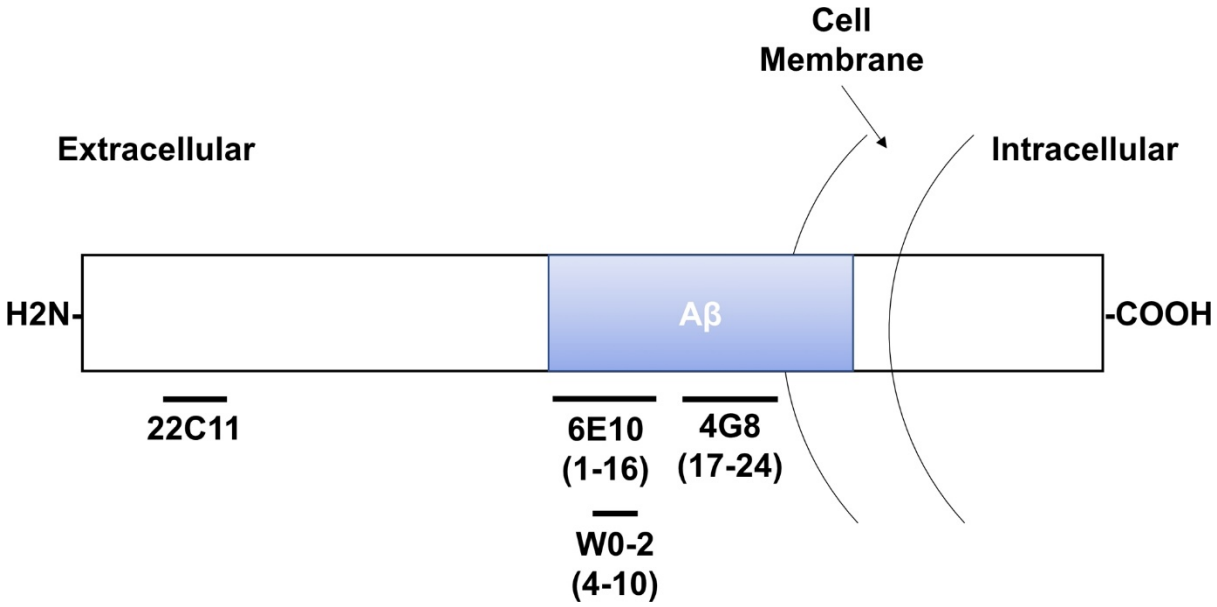
Cell
Membrane
Extracellular
Intracellular
H2N-
Aβ
-COOH
22C11
6E10
(1-16)
4G8
(17-24)
W0-2
(4-10)

Suppl. Fig. 2: Binding domains of anti-Aβ monoclonal antibodies. Diagram illustrating the binding domains of the antibodies used in this study, including anti-Aβ antibody W0-2, 6E10, and 4G8, which recognize amino acid residues (4-10), (1-16), and (17-24) of human Aβ, respectively. Antibody clone 22C11 recognizes amino acids (66-81) of the N-terminus on the amyloid precursor protein (APP).

Suppl. Fig. 3

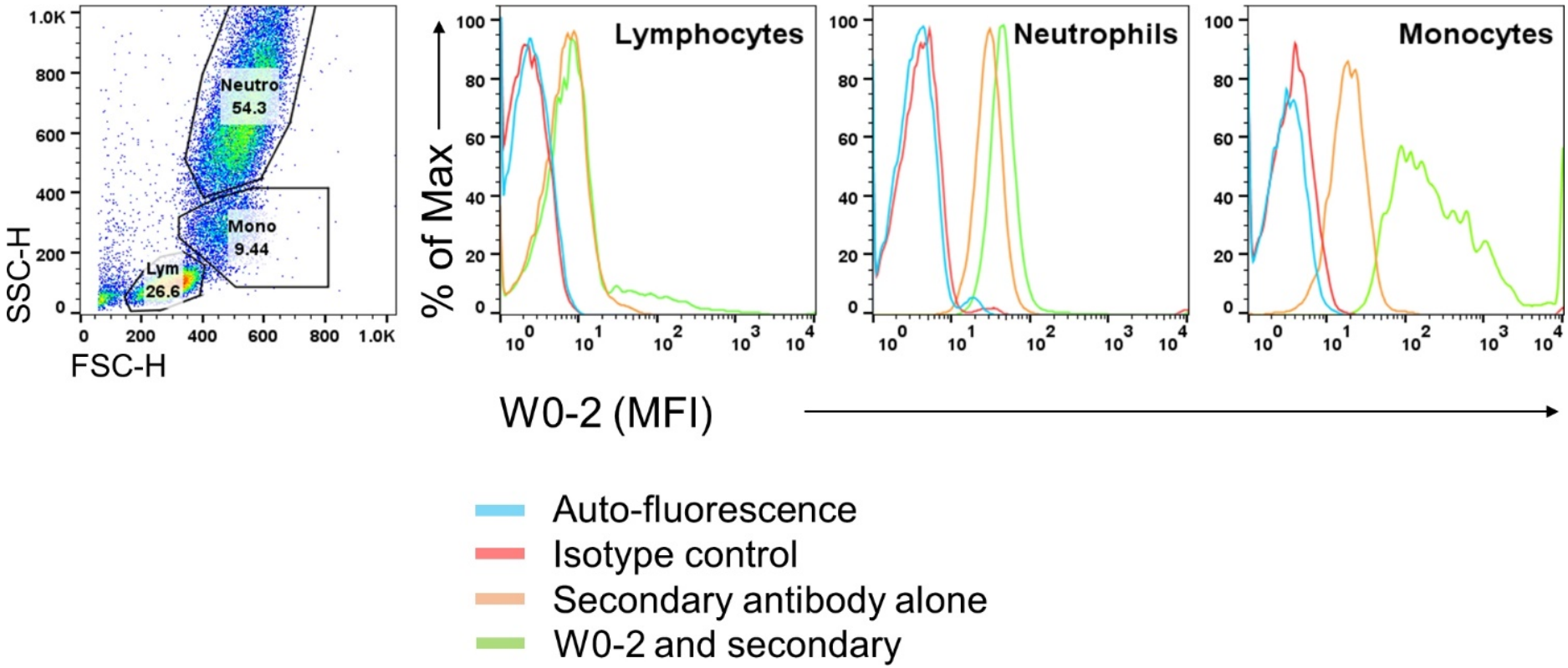
SSC-H
FSC-H
Neutro
54.3
Mono
9.44
Lym
26.6
% of Max
Lymphocytes
Neutrophils
Monocytes
W0-2 (MFI)
Auto-fluorescence
Isotype control
Secondary antibody alone
W0-2 and secondary

Suppl. Fig. 3: Flow cytometry histograms of Aβ peptide binding on human blood leukocytes. Typical flow cytometry histograms showing fluorescence intensity of the W0-2 and secondary antibody (% of Max), proportional to Aβ levels on cell surfaces after Aβ peptide binding by human blood leukocytes. Monocytes exhibited substantial Aβ peptide binding (n=6 blood samples, all CU), confirming Aβ peptide presence on monocyte cell surfaces.

Suppl. Fig. 4

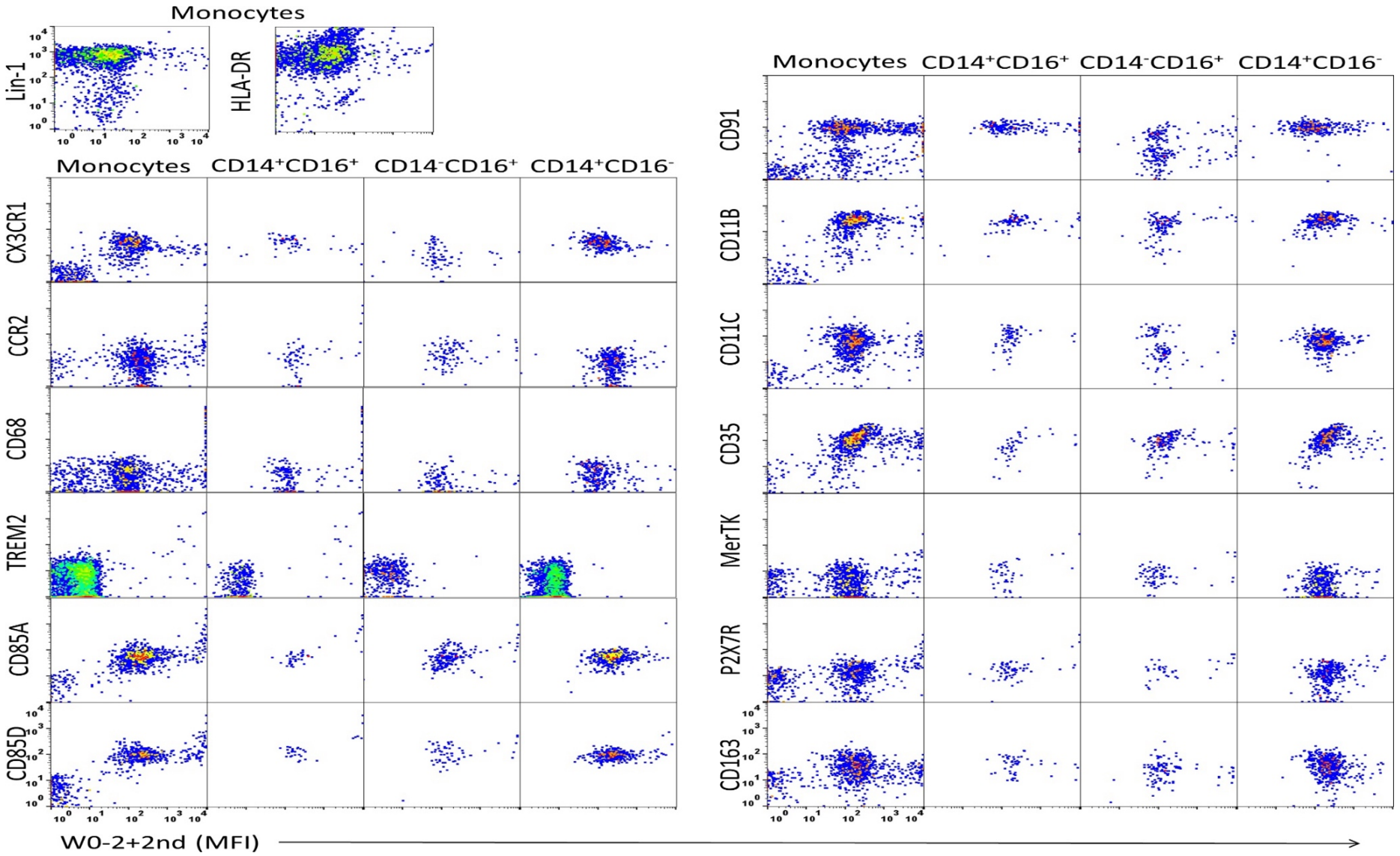
Monocytes
Lin-1
HLA-DR
Monocytes
CD14+CD16+
CD14-CD16+
CD14+CD16-
CX3CR1
CCR2
CD68
TREM2
CD85A
CD85D
Monocytes
CD14+CD16+
CD14-CD16+
CD14+CD16-
CD91
CD11B
CD11C
CD35
MerTK
P2X7R
CD163
W0-2+2nd (MFI)

Suppl. Fig. 4: Examining immune phenotyping characteristics of Aβ-binding monocyte subsets. Peripheral blood monocytes were initially gated based on forward and side scatter characteristics and further categorized according to the fluorescent intensity of CD14 and CD16. The Aβ-binding monocyte subsets were analyzed using four-color immunophenotypic analysis ($n \geqslant 3$, with a total of 22 blood samples analyzed). It is worth noting that in the four-color panel for TREM2, what matches TREM2, CD14, and CD16 was Qdot525 conjugated W0-2, not W0-2 plus secondary antibody. Across all biomarkers examined, the Aβ-binding monocytes within the three subsets exhibited similar immune phenotyping characteristics.

Suppl. Fig. 5

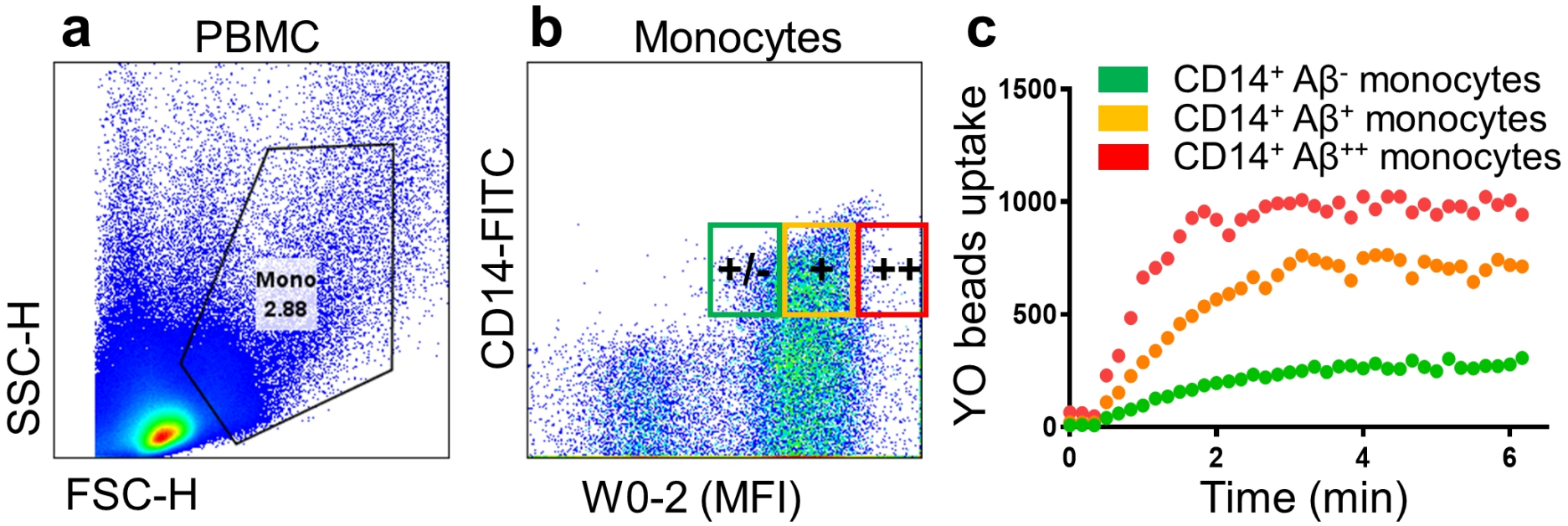
a
PBMC
Mono
2.88
SSC-H
FSC-H
b
Monocytes
+/-
+
++
CD14-FITC
W0-2 (MFI)
c
CD14+ Aβ- monocytes
CD14+ Aβ+ monocytes
CD14+ Aβ++ monocytes
YO beads uptake
1500
1000
500
0
0
2
4
6
Time (min)

Suppl. Fig. 5: Phagocytic activity of monocytes in relation to surface Aβ levels. To explore the link between surface Aβ levels on monocytes and their phagocytic function, three PBMCs from 1 CU, 1 MCI, and 1 AD-dementia were stained with W0-2 and secondary antibodies, followed with CD14 antibody. a-b. CD14+ monocytes were categorized into Aβ-, Aβ+, and Aβ++ subsets based on their surface Aβ levels. c. Phagocytic activity was assessed through real-time triple-color flow cytometry, measuring YO bead uptake. Results showed that CD14+Aβ++ monocytes exhibited the highest phagocytic activity, followed by CD14+Aβ+ monocytes, while CD14+Aβ- monocytes had the lowest uptake of YO beads.

Suppl. Fig. 6

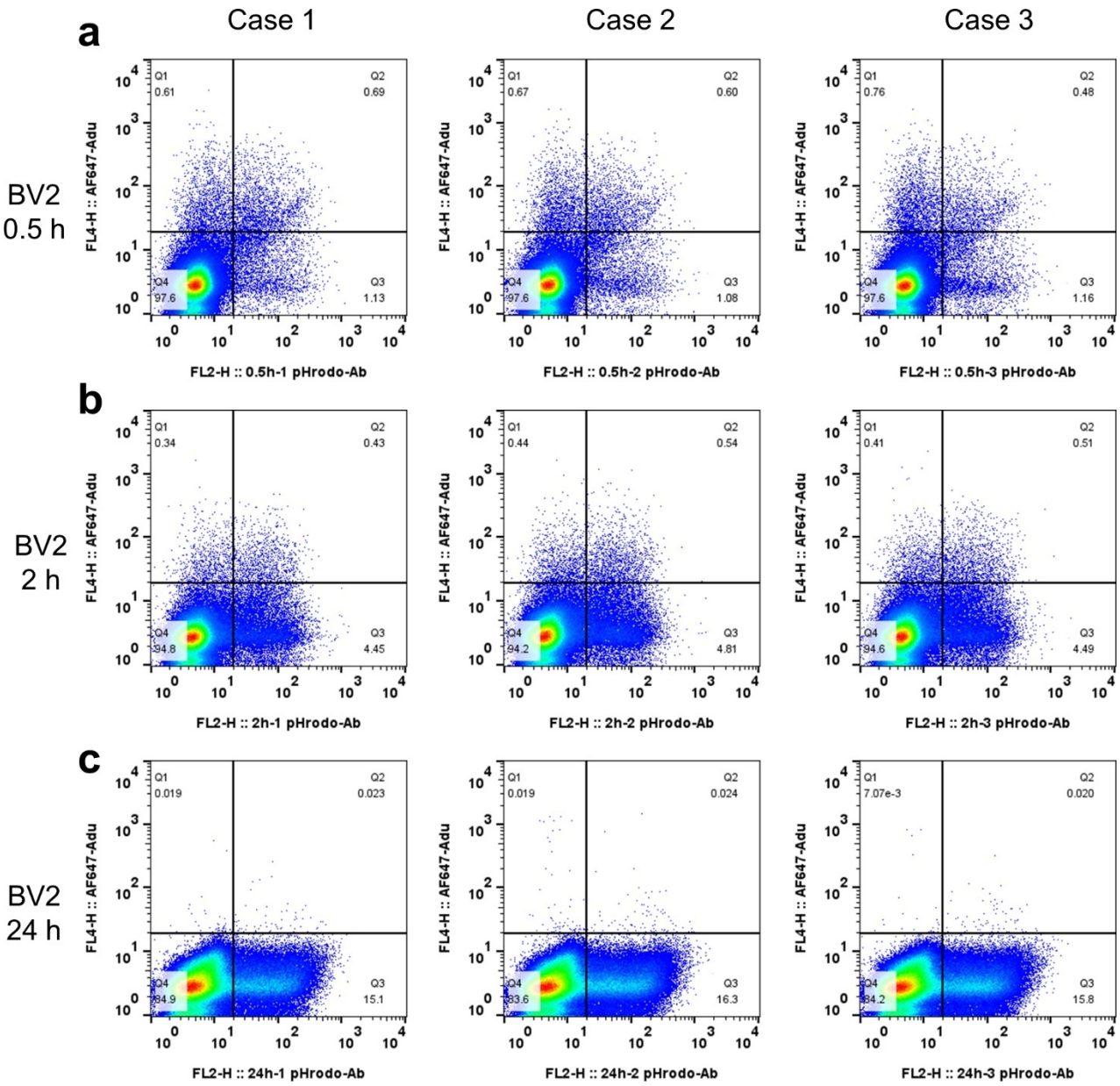
a
Case 1
Case 2
Case 3
BV2
0.5 h
b
BV2
2 h
c
BV2
24 h
FL4-H :: AF647-Adu
FL2-H :: 0.5h-1 pHrodo-Ab
FL2-H :: 0.5h-2 pHrodo-Ab
FL2-H :: 0.5h-3 pHrodo-Ab
FL2-H :: 2h-1 pHrodo-Ab
FL2-H :: 2h-2 pHrodo-Ab
FL2-H :: 2h-3 pHrodo-Ab
FL2-H :: 24h-1 pHrodo-Ab
FL2-H :: 24h-2 pHrodo-Ab
FL2-H :: 24h-3 pHrodo-Ab

Suppl. Fig. 6: Real-time monitoring of $A\beta_{1-42}$ phagocytosis by microglia using a Two-Color Fluorescent Reporting System. Real-time monitoring of $A\beta_{1-42}$ phagocytosis by microglia using a Two-Color Fluorescent Reporting System. A Two-Color Fluorescent Reporting System was built to monitor the uptake of $oA\beta_{1-42}$ by BV2 cells, utilizing AF647-conjugated Aducanumab (Adu) and pHrodo Red to visualize surface-bound and intra-lysosomal $oA\beta_{1-42}$. BV2 cells (n=3, in separate culture dishes) showed initial internalization of pHrodo-$oA\beta_{1-42}$ at 0.5 hours (Q3 in panel **a**), while a large amount of pHrodo-$oA\beta_{1-42}$ remained surface-bound (Q1 in panel **a**). BV2 cells showed substantial internalization of pHrodo-$oA\beta_{1-42}$ at 2 hours (Q3 in panel **b**), with still a substantial amount of pHrodo-$oA\beta_{1-42}$ surface-bound (Q1 in panel **b**). Most of the pHrodo-$oA\beta_{1-42}$ had been internalized by BV2 cells at 24 hours (Q3 in panel **c**), while a minimal amount of pHrodo-$oA\beta_{1-42}$ remained surface-bound (Q1 in panel **c**). Note that Q2 represents the BV2 cell subpopulation that has both surface-bound and internalized pHrodo-$oA\beta_{1-42}$.

Suppl. Fig. 7

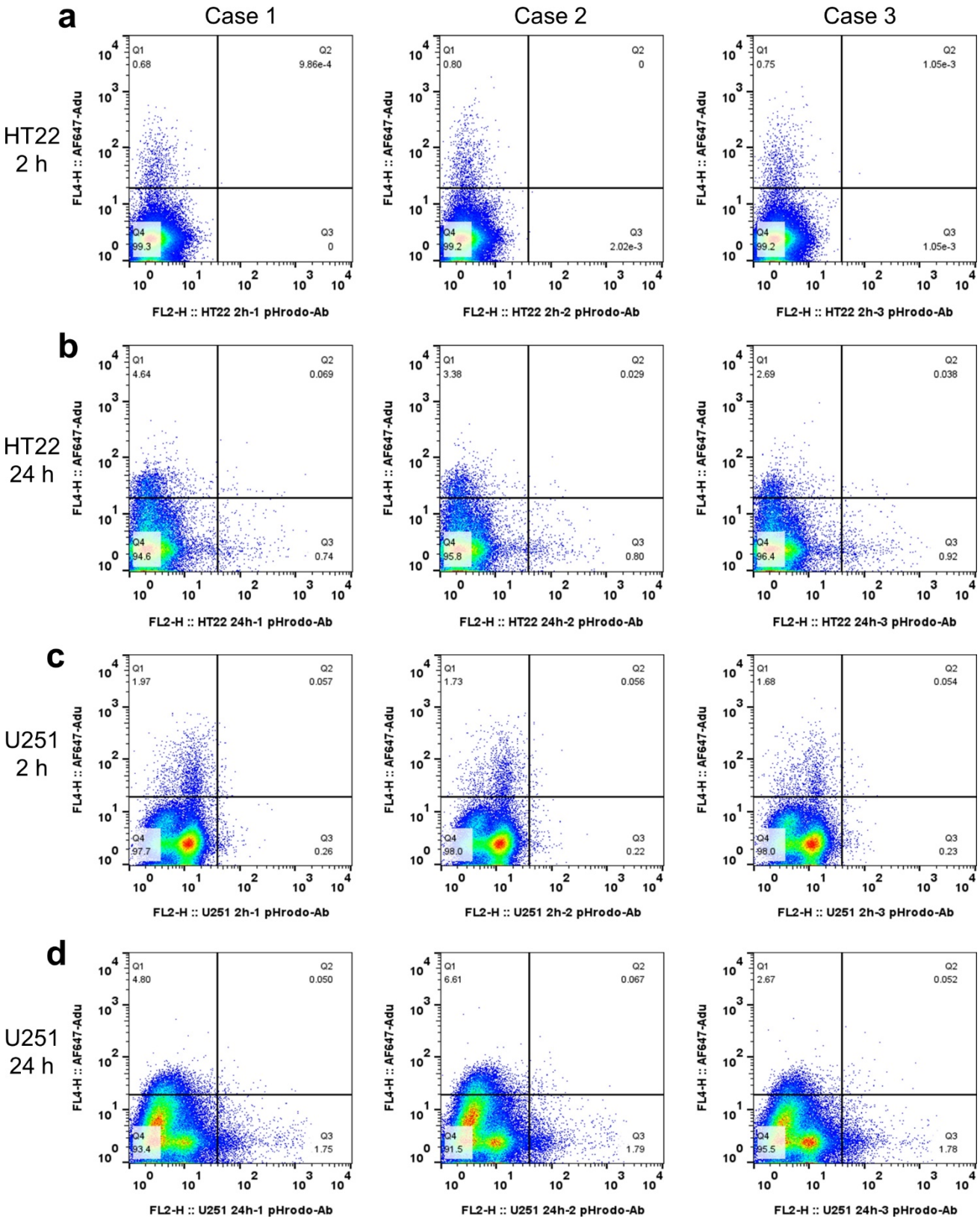
a
Case 1
Case 2
Case 3
HT22
2 h
Q1 0.68
Q2 9.86e-4
Q4 99.3
Q3 0
Q1 0.80
Q2 0
Q4 99.2
Q3 2.02e-3
Q1 0.75
Q2 1.05e-3
Q4 99.2
Q3 1.05e-3
FL4-H :: AF647-Adu
FL2-H :: HT22 2h-1 pHrodo-Ab
FL2-H :: HT22 2h-2 pHrodo-Ab
FL2-H :: HT22 2h-3 pHrodo-Ab
b
HT22
24 h
Q1 4.64
Q2 0.069
Q4 94.6
Q3 0.74
Q1 3.38
Q2 0.029
Q4 95.8
Q3 0.80
Q1 2.69
Q2 0.038
Q4 96.4
Q3 0.92
FL2-H :: HT22 24h-1 pHrodo-Ab
FL2-H :: HT22 24h-2 pHrodo-Ab
FL2-H :: HT22 24h-3 pHrodo-Ab
c
U251
2 h
Q1 1.97
Q2 0.057
Q4 97.7
Q3 0.26
Q1 1.73
Q2 0.056
Q4 98.0
Q3 0.22
Q1 1.68
Q2 0.054
Q4 98.0
Q3 0.23
FL2-H :: U251 2h-1 pHrodo-Ab
FL2-H :: U251 2h-2 pHrodo-Ab
FL2-H :: U251 2h-3 pHrodo-Ab
d
U251
24 h
Q1 4.80
Q2 0.050
Q4 93.4
Q3 1.75
Q1 6.61
Q2 0.067
Q4 91.5
Q3 1.79
Q1 2.67
Q2 0.052
Q4 95.5
Q3 1.78
FL2-H :: U251 24h-1 pHrodo-Ab
FL2-H :: U251 24h-2 pHrodo-Ab
FL2-H :: U251 24h-3 pHrodo-Ab

Suppl. Fig. 7: Real-time monitoring of $A\beta_{1-42}$ phagocytosis by neuronal and glial cells using a Two-Color Fluorescent Reporting System. A Two-Color Fluorescent Reporting System was developed to monitor the uptake of $oA\beta_{1-42}$ by HT22 and U251 cells, utilizing AF647-conjugated Aducanumab (Adu) and pHrodo Red to visualize surface-bound and intra-lysosomal $oA\beta_{1-42}$. Compared with BV2 cells, HT22 cells (n=3, in separate culture dishes) displayed surface adhesion without subsequent internalization after 2 hours (**a**) and showed weak internalization after 24 hours (**b**). In contrast, U251 cells (n=3, in separate culture dishes) exhibited surface adhesion with weak internalization after 2 hours (**c**), which became more apparent after 24 hours (**d**).

Suppl. Fig. 8

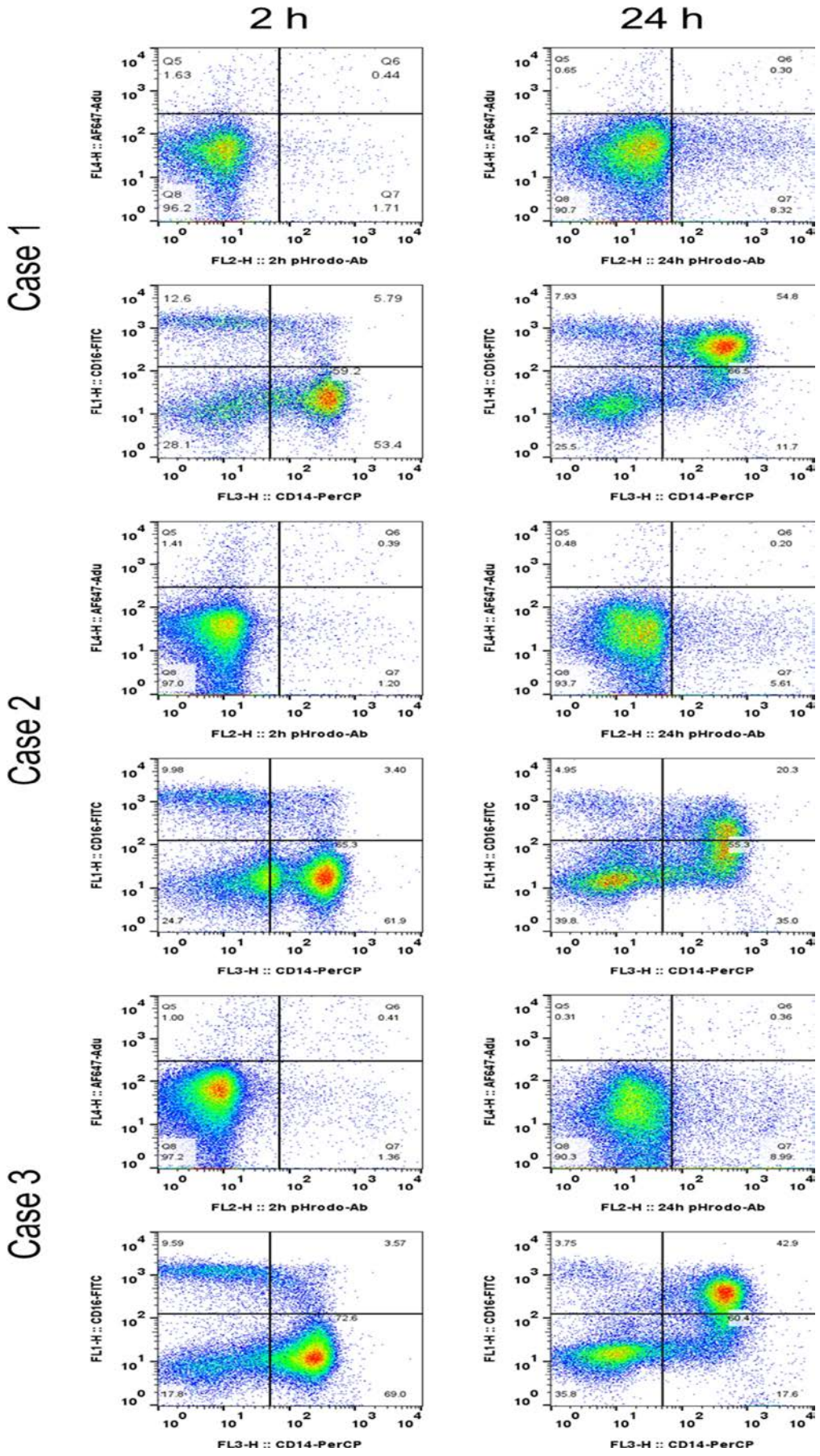
2 h
24 h
Case 1
Case 2
Case 3
FL4-H :: AF647-Adu
FL2-H :: 2h pHrodo-Ab
FL2-H :: 24h pHrodo-Ab
FL1-H :: CD16-FITC
FL3-H :: CD14-PerCP
Q5 1.63
Q6 0.44
Q8 96.2
Q7 1.71
Q5 0.65
Q6 0.30
Q8 90.7
Q7 8.32
12.6
5.79
59.2
28.1
53.4
7.93
54.8
25.5
11.7
Q5 1.41
Q6 0.39
Q8 97.0
Q7 1.20
Q5 0.48
Q6 0.20
Q8 93.7
Q7 5.61
9.98
3.40
65.3
24.7
61.9
4.95
20.3
39.8
35.0
Q5 1.00
Q6 0.41
Q8 97.2
Q7 1.36
Q5 0.31
Q6 0.36
Q8 90.3
Q7 8.99
9.59
3.57
72.6
17.8
69.0
3.75
42.9
35.8
17.6

Suppl. Fig. 8: Real-time monitoring of $A\beta_{1-42}$ phagocytosis by monocytes using a Two-Color Fluorescent Reporting System. Using AF647-conjugated Aducanumab (Adu) and pHrodo red to visualize surface-bound and intra-lysosomal $oA\beta_{1-42}$, a Two-Color Fluorescent Reporting System was built to monitor the uptake of $oA\beta_{1-42}$ by monocytes. Human PBMCs, including monocytes from three individuals (1 CU, 1 MCI, and 1 AD-dementia), exhibited substantial internalization of pHrodo-oAβ1-42 after 24 hours; Classic monocytes ($CD14^+CD16^-$) differentiated into intermediate monocytes ($CD14^+CD16^+$) after treatment, indicating a pro-inflammatory response.

Suppl. Fig. 9

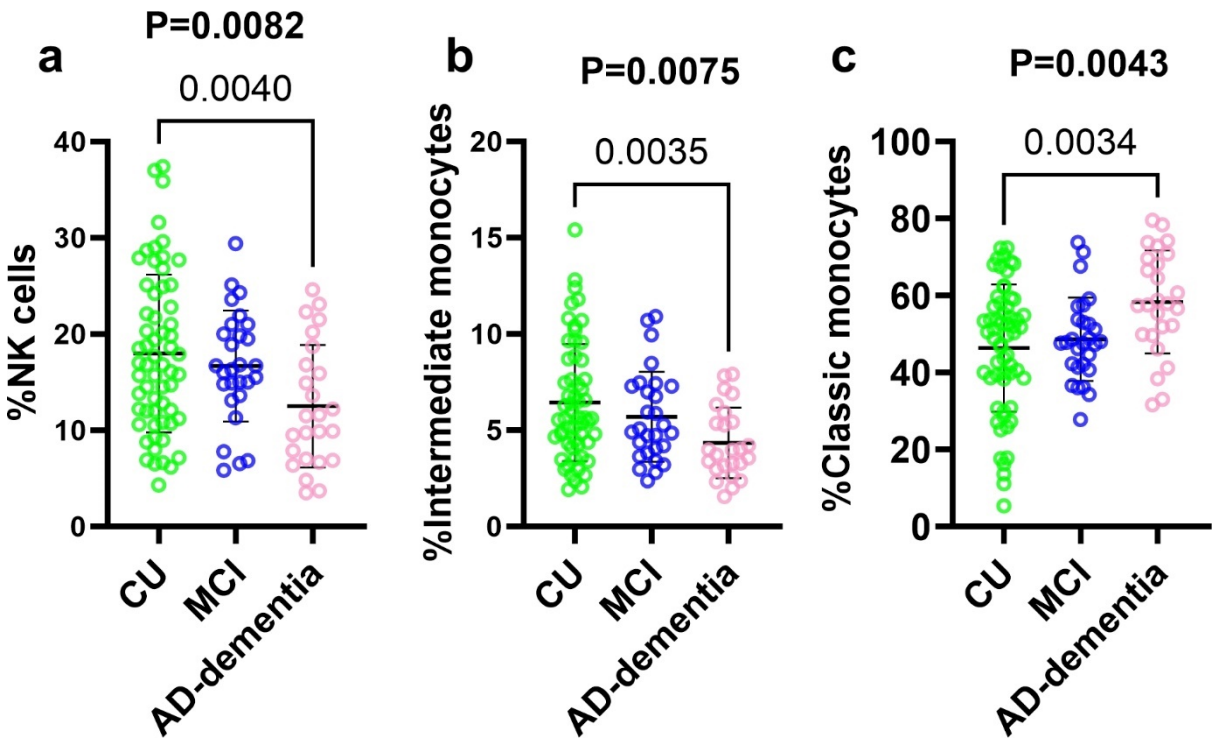
a
P=0.0082
0.0040
%NK cells
40
30
20
10
0
CU
MCI
AD-dementia
b
P=0.0075
0.0035
%Intermediate monocytes
20
15
10
5
0
CU
MCI
AD-dementia
c
P=0.0043
0.0034
%Classic monocytes
100
80
60
40
20
0
CU
MCI
AD-dementia

Suppl. Fig. 9: Correlations between alterations in lymphocyte and monocytic subsets percentages and AD clinical stages. Compared to CU (n=64), the percentages of NK cells (**a**) and $CD14^{+}CD16^{+}$ intermediate monocytes (**b**) reduced in MCI/AD-dementia (n=25, 24). Conversely, the percentage of $CD14^{+}CD16^{-}$ classical monocytes elevated in MCI/AD-dementia compared to CU (**c**). The column dot plots represent mean ± standard deviation. The datasets were not normally distributed, and P values were determined using the Kruskal-Wallis test, followed by Dunn's multiple comparisons test (solid zig-zag line). Notably, a one-way ordinary ANOVA test was applied to %NK cells due to the normal distribution of the data.

Suppl. Fig. 10

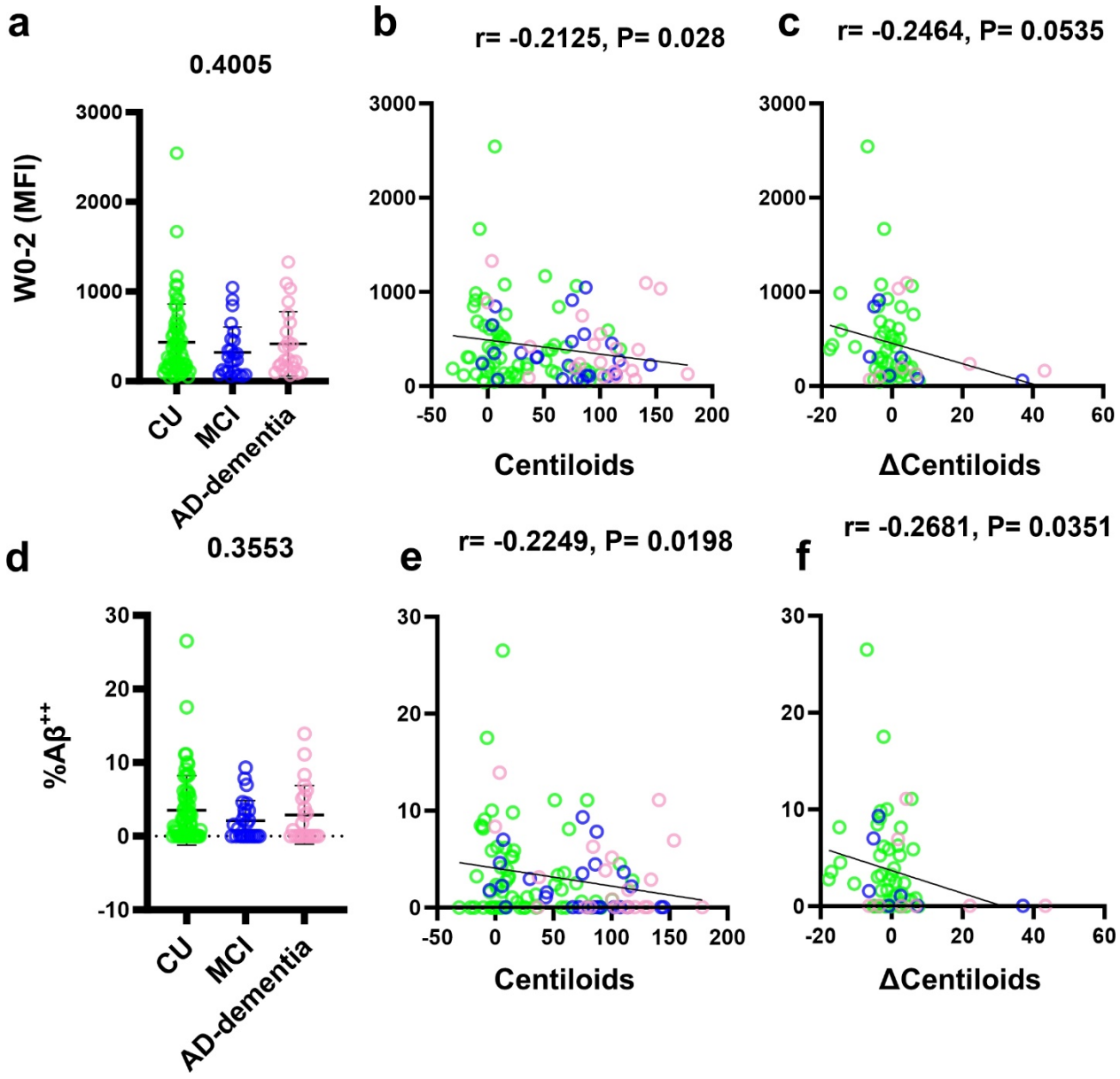
a
0.4005
W0-2 (MFI)
3000
2000
1000
0
CU
MCI
AD-dementia
b
r= -0.2125, P= 0.028
Centiloids
c
r= -0.2464, P= 0.0535
ΔCentiloids
d
0.3553
%Aβ++
30
20
10
0
-10
e
r= -0.2249, P= 0.0198
f
r= -0.2681, P= 0.0351

Suppl. Fig. 10: Monocyte subset - Intermediate Monocyte - surface Aβ and their associations with AD clinical stages, brain Aβ-PET burden and annual progression of Aβ-PET burden. The relationship between intermediate monocyte surface Aβ (including fluorescence intensity and the percentage of $A\beta^{++}$ monocytes) and the clinical stages of AD (**a** & **d**), brain Aβ-PET burden (**b** & **e**) and the annual progression of brain Aβ-PET burden (ΔCentiloid, **c** & **f**) was investigated in 113 participants (64 CU, 25 MCI, and 24 AD-Dementia). The column dot plots illustrate the mean ± standard deviation, and the P values were determined through the Kruskal-Wallis test followed by Dunn's multiple comparisons test (solid zig-zag line). If a test was not statistically significant, only the Kruskal-Wallis P value was shown. Correlation coefficients (r) and P values were calculated using Spearman correlation analysis.

Suppl. Fig. 11

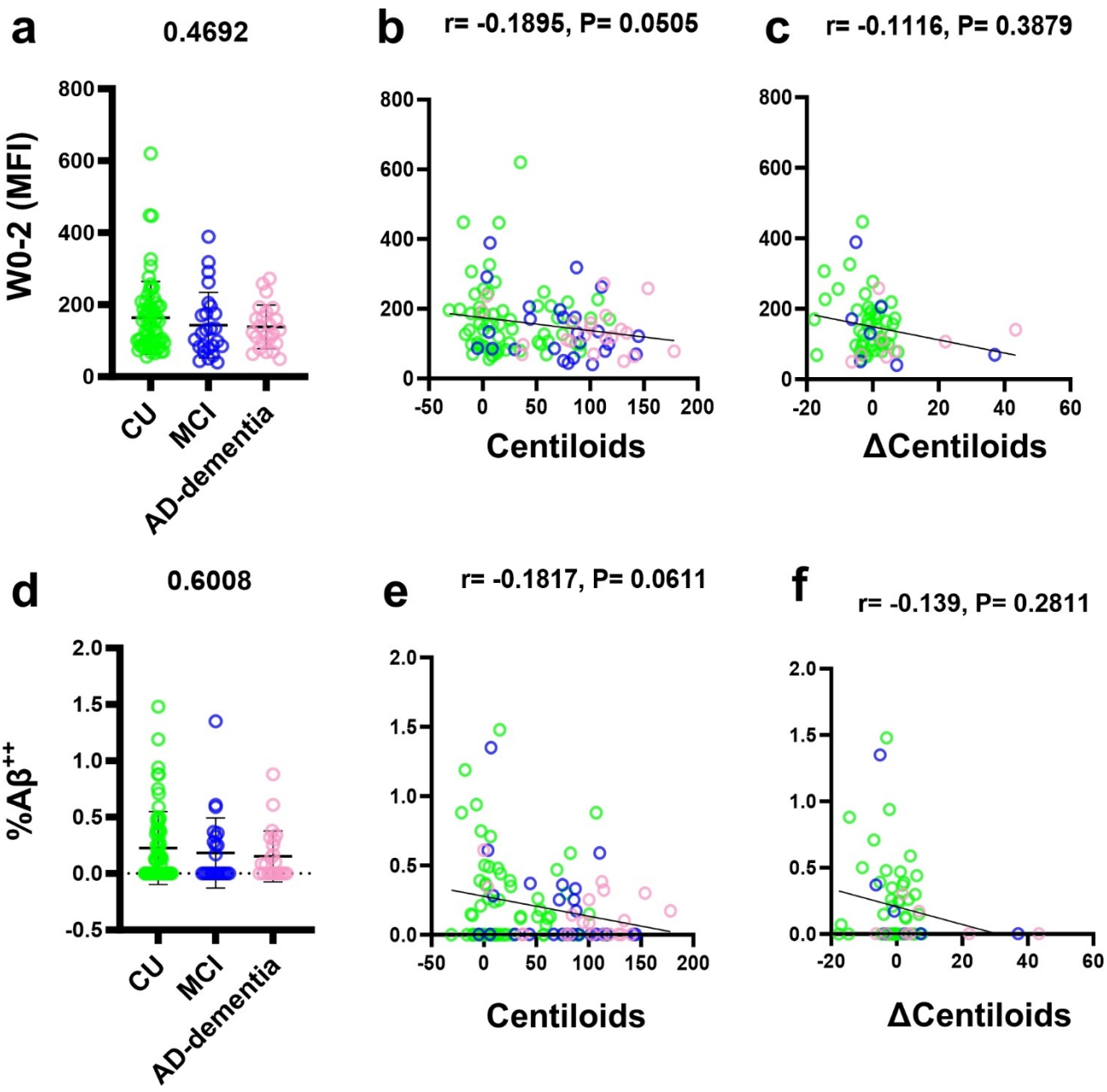
a
0.4692
W0-2 (MFI)
800
600
400
200
0
CU
MCI
AD-dementia
b
r= -0.1895, P= 0.0505
800
600
400
200
0
-50
0
50
100
150
200
Centiloids
c
r= -0.1116, P= 0.3879
800
600
400
200
0
-20
0
20
40
60
ΔCentiloids
d
0.6008
%Aβ++
2.0
1.5
1.0
0.5
0.0
-0.5
CU
MCI
AD-dementia
e
r= -0.1817, P= 0.0611
2.0
1.5
1.0
0.5
0.0
-50
0
50
100
150
200
Centiloids
f
r= -0.139, P= 0.2811
2.0
1.5
1.0
0.5
0.0
-20
0
20
40
60
ΔCentiloids

Suppl. Fig. 11: Monocyte subset - Classic Monocyte - surface Aβ and their associations with AD clinical stages, brain Aβ-PET burden and annual progression of Aβ-PET burden. The relationship between classical monocyte surface Aβ (including fluorescence intensity and the percentage of $A\beta^{++}$ monocytes) and the clinical stages of AD (**a** & **d**), brain Aβ-PET burden (**b** & **e**) and the annual progression of brain Aβ-PET burden (ΔCentiloid, **c** & **f**) was investigated in 113 participants (64 CU, 25 MCI, and 24 AD-Dementia). The column dot plots illustrate the mean ± standard deviation, and the P values were determined through the Kruskal-Wallis test followed by Dunn's multiple comparisons test (solid zig-zag line). If a test was not statistically significant, only the Kruskal-Wallis P value was shown. Correlation coefficients (r) and P values were calculated using Spearman correlation analysis.

Suppl. Fig. 12

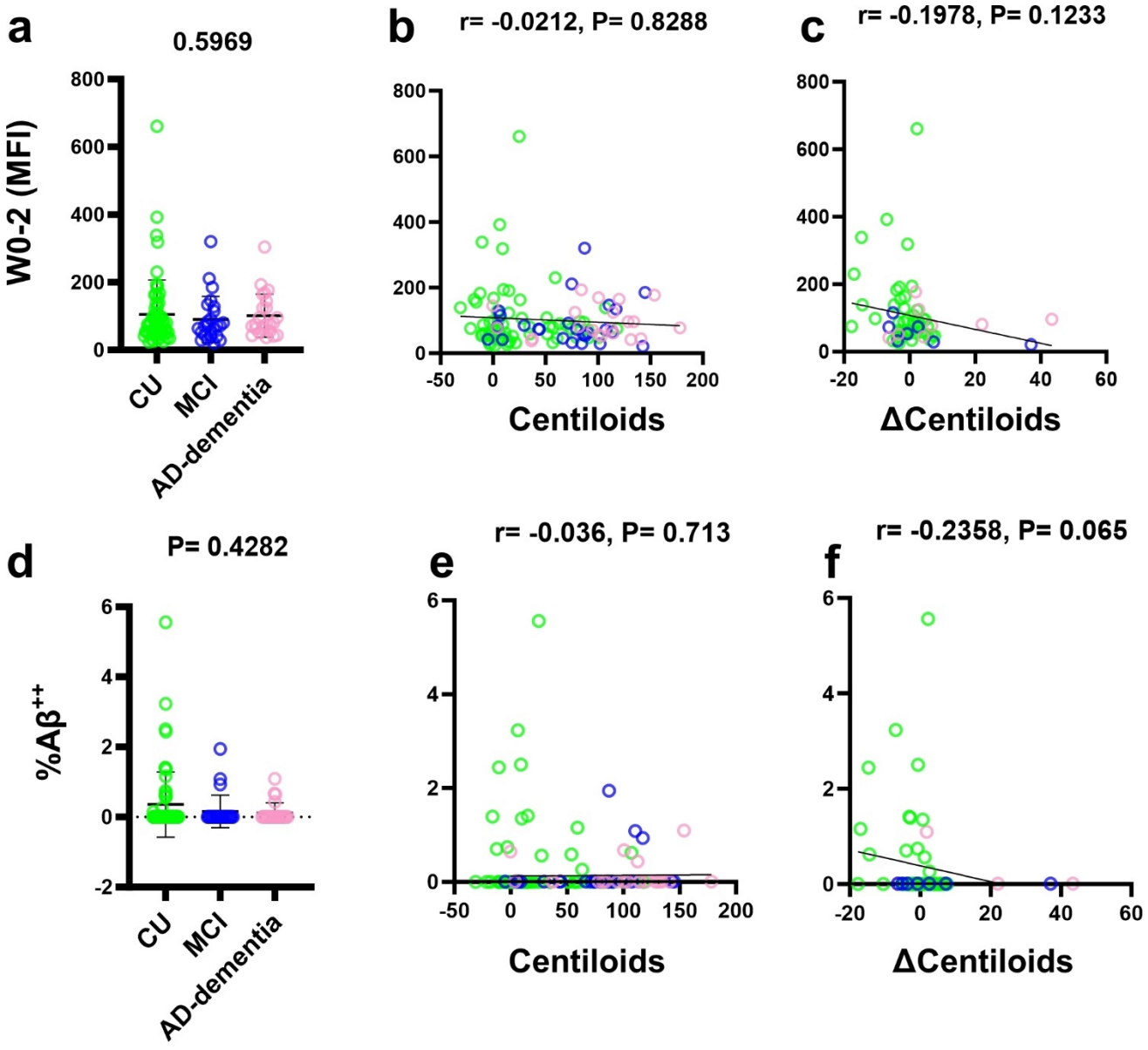
a
0.5969
W0-2 (MFI)
800
600
400
200
0
CU
MCI
AD-dementia
b
r= -0.0212, P= 0.8288
800
600
400
200
0
-50
0
50
100
150
200
Centiloids
c
r= -0.1978, P= 0.1233
800
600
400
200
0
-20
0
20
40
60
ΔCentiloids
d
P= 0.4282
%Aβ++
6
4
2
0
-2
CU
MCI
AD-dementia
e
r= -0.036, P= 0.713
6
4
2
0
-50
0
50
100
150
200
Centiloids
f
r= -0.2358, P= 0.065
6
4
2
0
-20
0
20
40
60
ΔCentiloids

Suppl. Fig. 12: Monocyte subset - Non-classic Monocyte - surface Aβ and their associations with AD clinical stages, brain Aβ-PET burden and annual progression of Aβ-PET burden. The relationship between non-classical monocyte surface Aβ (including fluorescence intensity and the percentage of $A\beta^{++}$ monocytes) and the clinical stages of AD (**a** & **d**), brain Aβ-PET burden (**b** & **e**) and the annual progression of brain Aβ-PET burden (ΔCentiloid, **c** & **f**) was investigated in 113 participants (64 CU, 25 MCI, and 24 AD-Dementia). The column dot plots illustrate the mean ± standard deviation, and the P values were determined through the Kruskal-Wallis test followed by Dunn's multiple comparisons test (solid zig-zag line). If a test was not statistically significant, only the Kruskal-Wallis P value was shown. Correlation coefficients (r) and P values were calculated using Spearman correlation analysis.

Suppl. Fig. 13

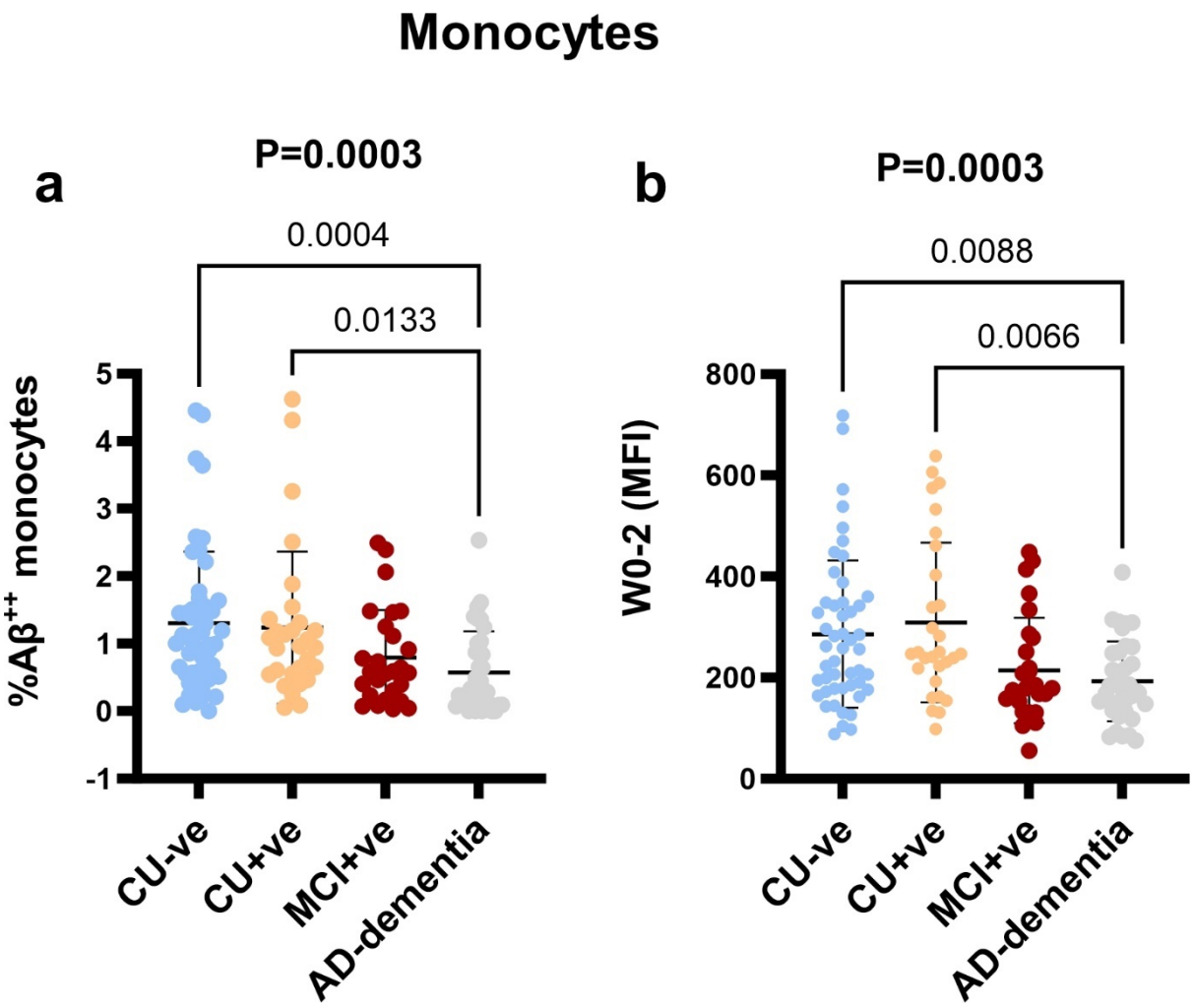
Monocytes
a
P=0.0003
0.0004
0.0133
%Aβ++ monocytes
5
4
3
2
1
0
-1
CU-ve
CU+ve
MCI+ve
AD-dementia
b
P=0.0003
0.0088
0.0066
W0-2 (MFI)
800
600
400
200
0
CU-ve
CU+ve
MCI+ve
AD-dementia

Suppl. Fig. 13: Monocyte surface Aβ Changes in Aβ-PET+ CU Individuals. CU individuals were compared based on brain Aβ-PET status (CU-ve: n=49; CU+ve: n=29), MCI+ve (n=27), and AD-dementia (n=36), with exclusion of MCI-ve participants (n=9) from the comparison. **Panel a**: It was found that CU+ve individuals exhibited a lower percentage of $A\beta^{++}$ monocytes compared to CU-ve individuals, but the difference was not statistically significant. Additionally, slightly elevated surface Aβ fluorescent intensity was observed in CU+ve compared to CU-ve individuals, but the difference was not statistically significant either, as shown in **Panel b**. The column dot plots represent mean ± standard deviation. Group comparison was determined by Kruskal-Wallis test followed by Dunn's multiple comparisons test (solid zig-zag line). If a test was not statistically significant, only a Kruskal-Wallis P value was shown.

Suppl. Fig. 14

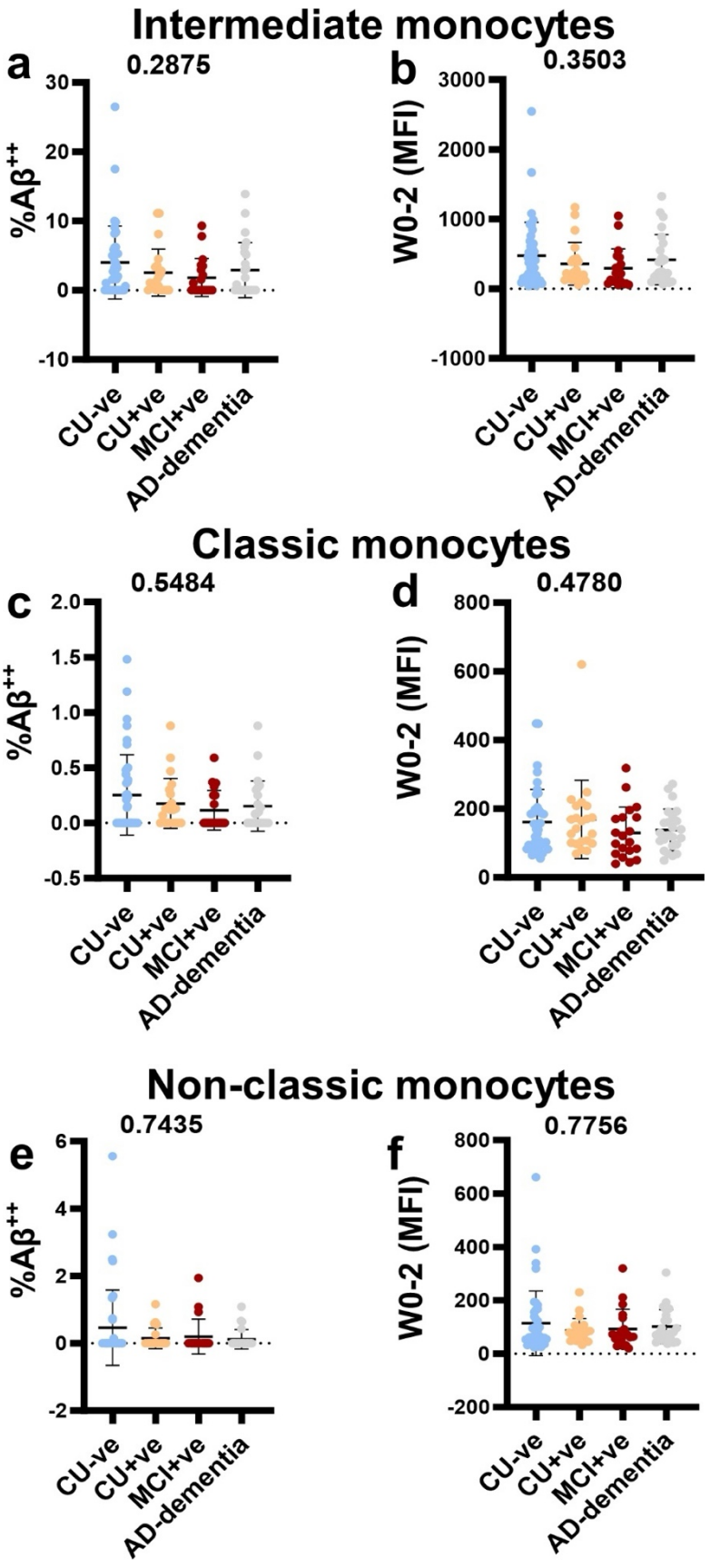
Intermediate monocytes
a
0.2875
%Aβ++
30
20
10
0
-10
CU-ve
CU+ve
MCI+ve
AD-dementia
b
0.3503
W0-2 (MFI)
3000
2000
1000
0
-1000
CU-ve
CU+ve
MCI+ve
AD-dementia
Classic monocytes
c
0.5484
%Aβ++
2.0
1.5
1.0
0.5
0.0
-0.5
CU-ve
CU+ve
MCI+ve
AD-dementia
d
0.4780
W0-2 (MFI)
800
600
400
200
0
CU-ve
CU+ve
MCI+ve
AD-dementia
Non-classic monocytes
e
0.7435
%Aβ++
6
4
2
0
-2
CU-ve
CU+ve
MCI+ve
AD-dementia
f
0.7756
W0-2 (MFI)
800
600
400
200
0
-200
CU-ve
CU+ve
MCI+ve
AD-dementia

Suppl. Fig. 14: Surface Aβ Changes of monocytic subsets in Aβ-PET+ CU Individuals. CU individuals were compared based on brain Aβ-PET status (CU-ve: n=49; CU+ve: n=29), MCI+ve (n=27), and AD-dementia (n=36), with exclusion of MCI-ve participants (n=9) from the comparison. The data is presented across three monocytic subsets. **Panels a, c, e**: These panels demonstrate that CU+ve individuals have a lower percentage of $A\beta^{++}$ monocytes compared to CU-ve individuals, with the percentage being similar to that observed in MCI+ve and AD-dementia individuals. This trend is consistent across all three monocyte subsets. In contrast, **Panel d** shows that CU+ve individuals exhibit a slight elevation in surface Aβ fluorescent intensity compared to CU-ve individuals within the classic monocyte subset. However, this increase in surface Aβ fluorescent intensity is not observed in the CU+ve groups within the intermediate and non-classic monocyte subsets, as shown in **Panels b, f**. The column dot plots represent mean ± standard deviation. Group comparison was determined by Kruskal-Wallis test followed by Dunn's multiple comparisons test (solid zig-zag line). If a test was not statistically significant, only a Kruskal-Wallis P value was shown.

Suppl. Fig. 15

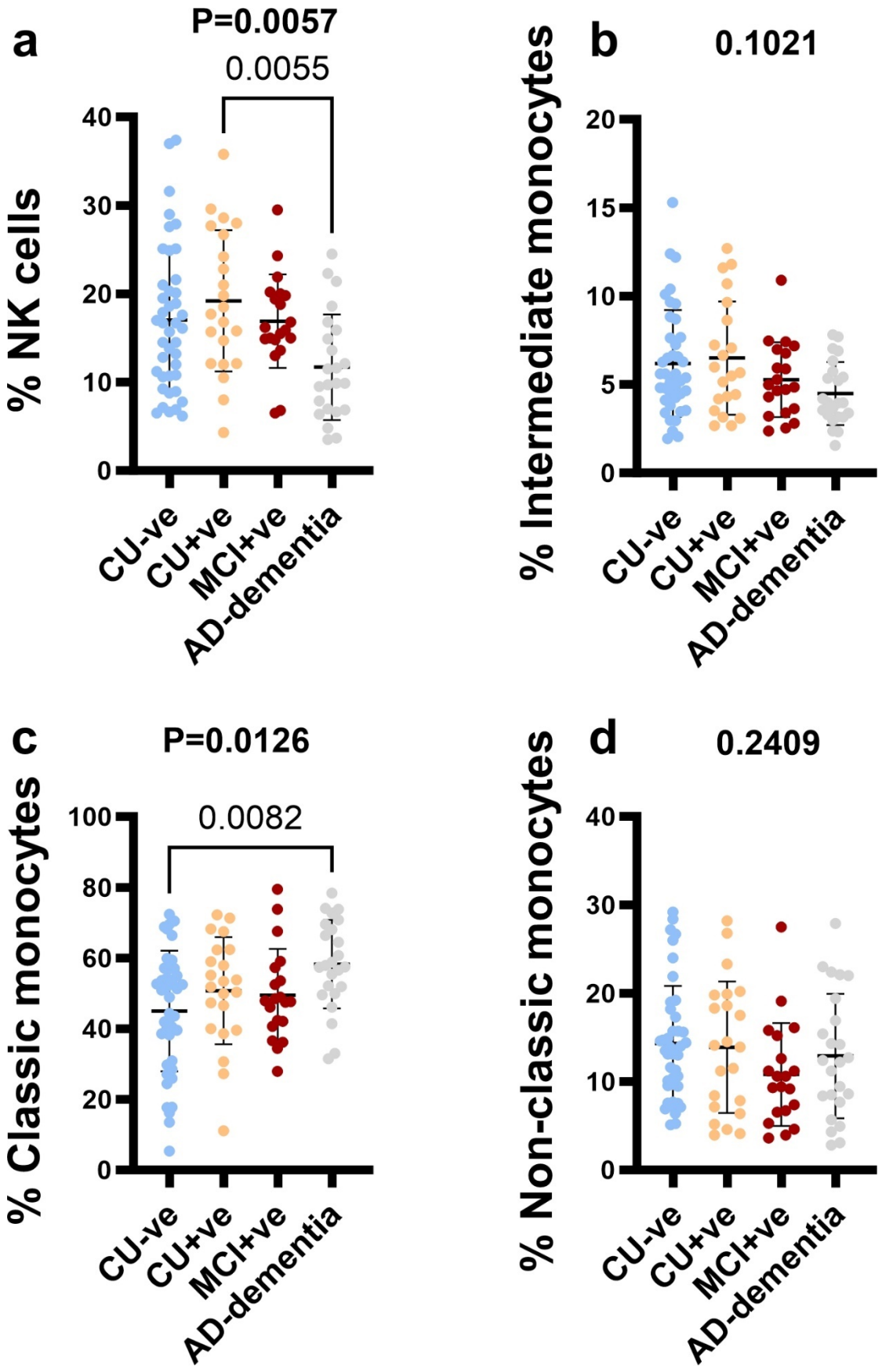
a
P=0.0057
0.0055
% NK cells
40
30
20
10
0
CU-ve
CU+ve
MCI+ve
AD-dementia
b
0.1021
% Intermediate monocytes
20
15
10
5
0
CU-ve
CU+ve
MCI+ve
AD-dementia
c
P=0.0126
0.0082
% Classic monocytes
100
80
60
40
20
0
CU-ve
CU+ve
MCI+ve
AD-dementia
d
0.2409
% Non-classic monocytes
40
30
20
10
0
CU-ve
CU+ve
MCI+ve
AD-dementia

Suppl. Fig. 15: Percentage Changes of NK Cells and Monocytic Subsets in Aβ-PET+ CU Individuals. CU individuals were compared based on brain Aβ-PET status (CU-ve: n=49; CU+ve: n=29), MCI+ve (n=27), and AD-dementia (n=36), with exclusion of MCI-ve participants (n=9) from the comparison. **Panel a**: CU+ve individuals showed a higher percentage of NK cells than CU-ve individuals. **Panel c:** The percentage of classic monocytes is slightly elevated in CU+ve individuals compared to CU-ve individuals, but the difference is not statistically significant. **Panel b, d:** There are no apparent differences between CU+ve and CU-ve individuals in the percentage of intermediate monocytes or non-classic monocytes. The column dot plots represent mean ± standard deviation. Group comparison was determined by Kruskal-Wallis test followed by Dunn's multiple comparisons test (solid zig-zag line). If a test was not statistically significant, only a Kruskal-Wallis P value was shown.

Suppl. Fig. 16

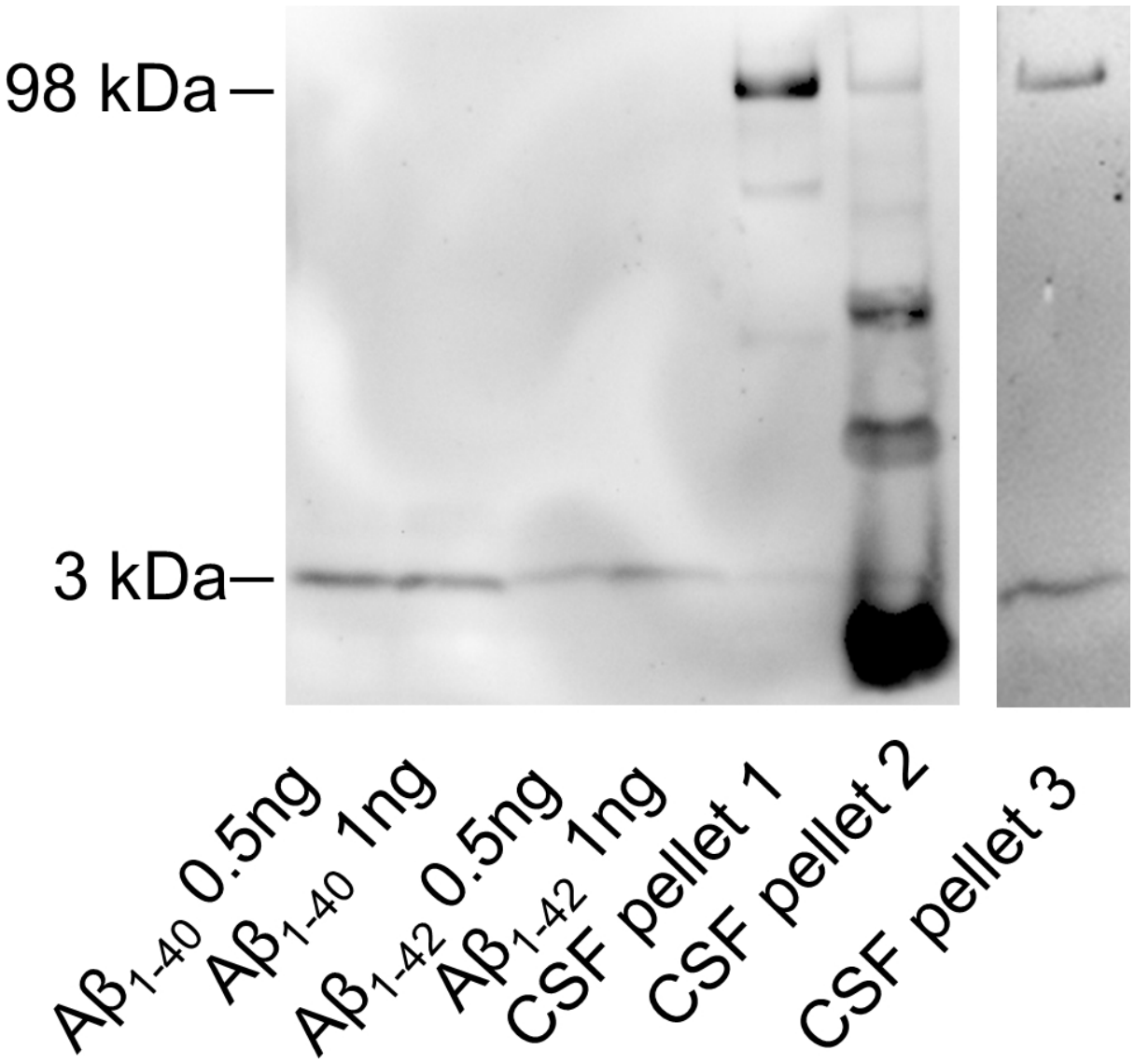
98 kDa
3 kDa
Aβ1-40 0.5ng
Aβ1-40 1ng
Aβ1-42 0.5ng
Aβ1-42 1ng
CSF pellet 1
CSF pellet 2
CSF pellet 3

Suppl. Fig. 16: Western blot detection of Aβ peptides on CSF pellet cells. Western blot demonstrated the presence of Aβ peptides in three CSF pellet cell samples of two blots.

Suppl. Fig. 17

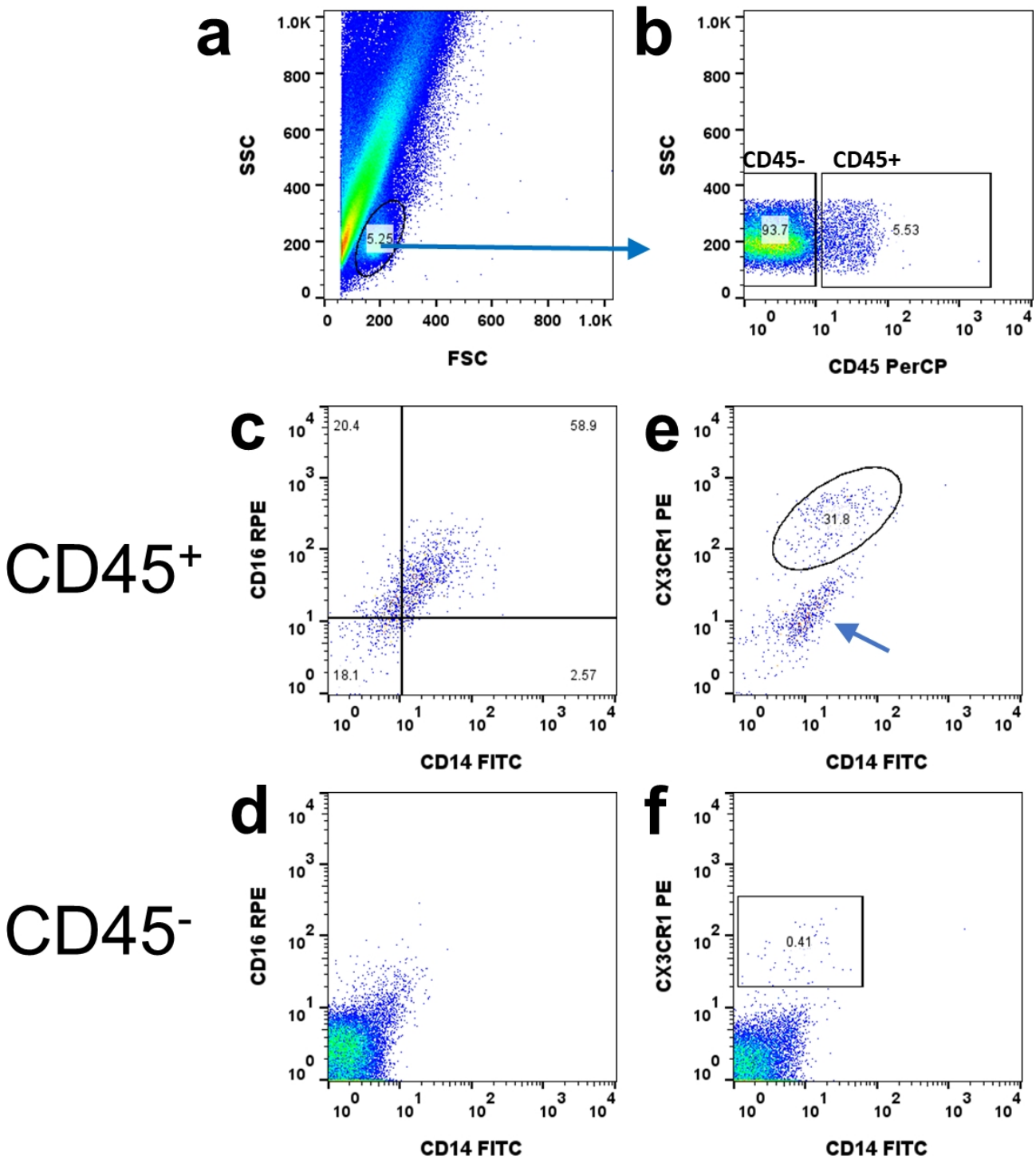
a
SSC
FSC
5.25
b
SSC
CD45-
CD45+
93.7
5.53
CD45 PerCP
CD45+
c
CD16 RPE
20.4
58.9
18.1
2.57
CD14 FITC
e
CX3CR1 PE
31.8
CD14 FITC
CD45-
d
CD16 RPE
CD14 FITC
f
CX3CR1 PE
0.41
CD14 FITC

Suppl. Fig. 17: Characterization of CSF monocyte entry into the brain. To explore the potential entry of CSF monocytes into the brain, post-mortem brain samples from two motor neuron disease patients were examined (n=3, 1 patient with front cortex and temporal cortex, the other with temporal cortex only). **a-b.** Brain cells were initially discriminated from myelin based on forward and side scatter characteristics, and further categorized according to the fluorescent intensity of CD45. **c.** Initial findings confirmed the presence of $CD45^{+}CD14^{+}CD16^{+}$ monocytes in the examined brain samples. **d.** $CD45^{-}$ brain cells were $CD14^{-}CD16^{-}$. **e.** Due to high levels of autofluorescence in brain cells (arrow pointed), additional marker such as CX3CR1 was used to distinguish the brain monocytes (circled). **f.** A subset of $CD45^{-}$ brain cells expressed CX3CR1, indicating their potential classification as microglia (marked in squares).

Suppl. Fig. 18

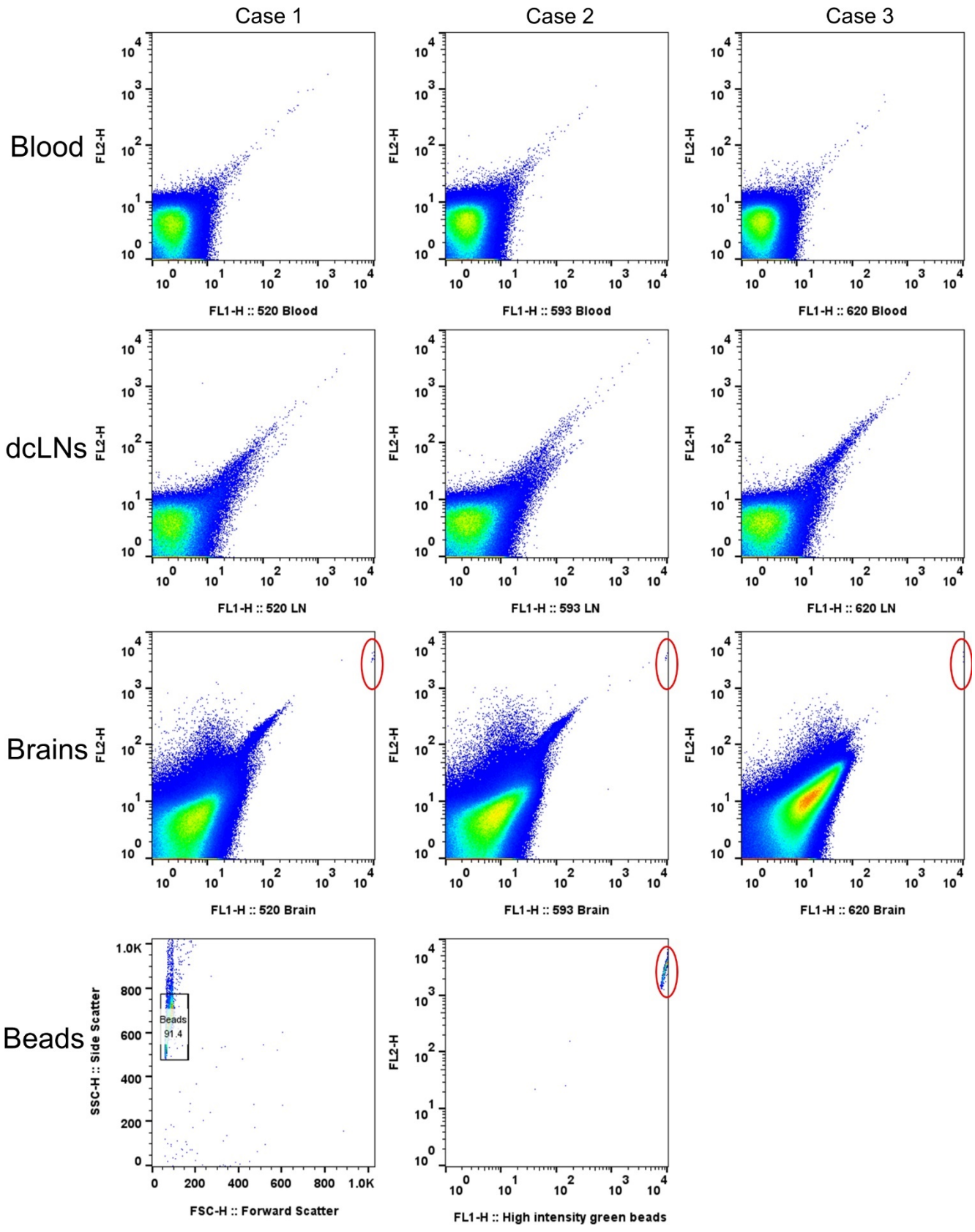
Case 1
Case 2
Case 3
Blood
dcLNs
Brains
Beads
FL2-H
FL1-H :: 520 Blood
FL1-H :: 593 Blood
FL1-H :: 620 Blood
FL1-H :: 520 LN
FL1-H :: 593 LN
FL1-H :: 620 LN
FL1-H :: 520 Brain
FL1-H :: 593 Brain
FL1-H :: 620 Brain
SSC-H :: Side Scatter
FSC-H :: Forward Scatter
Beads
91.4
FL1-H :: High intensity green beads

Suppl. Fig. 18: Validation of Physiological Cell Migration Using Bead Control in APP/PS1 Mice. 6 µm high-intensity alignment green beads were injected into the lateral ventricle of three APP/PS1 mice as a control study. Two days post-injection, peripheral blood and dcLNs were collected to trace the beads, with no detection in circulation or lymph nodes, confirming physiological cell migration. The beads were analyzed based on forward and side scatter characteristics and further categorized according to the fluorescent intensity.

Uncropped scan 1 for Suppl. Fig. 16

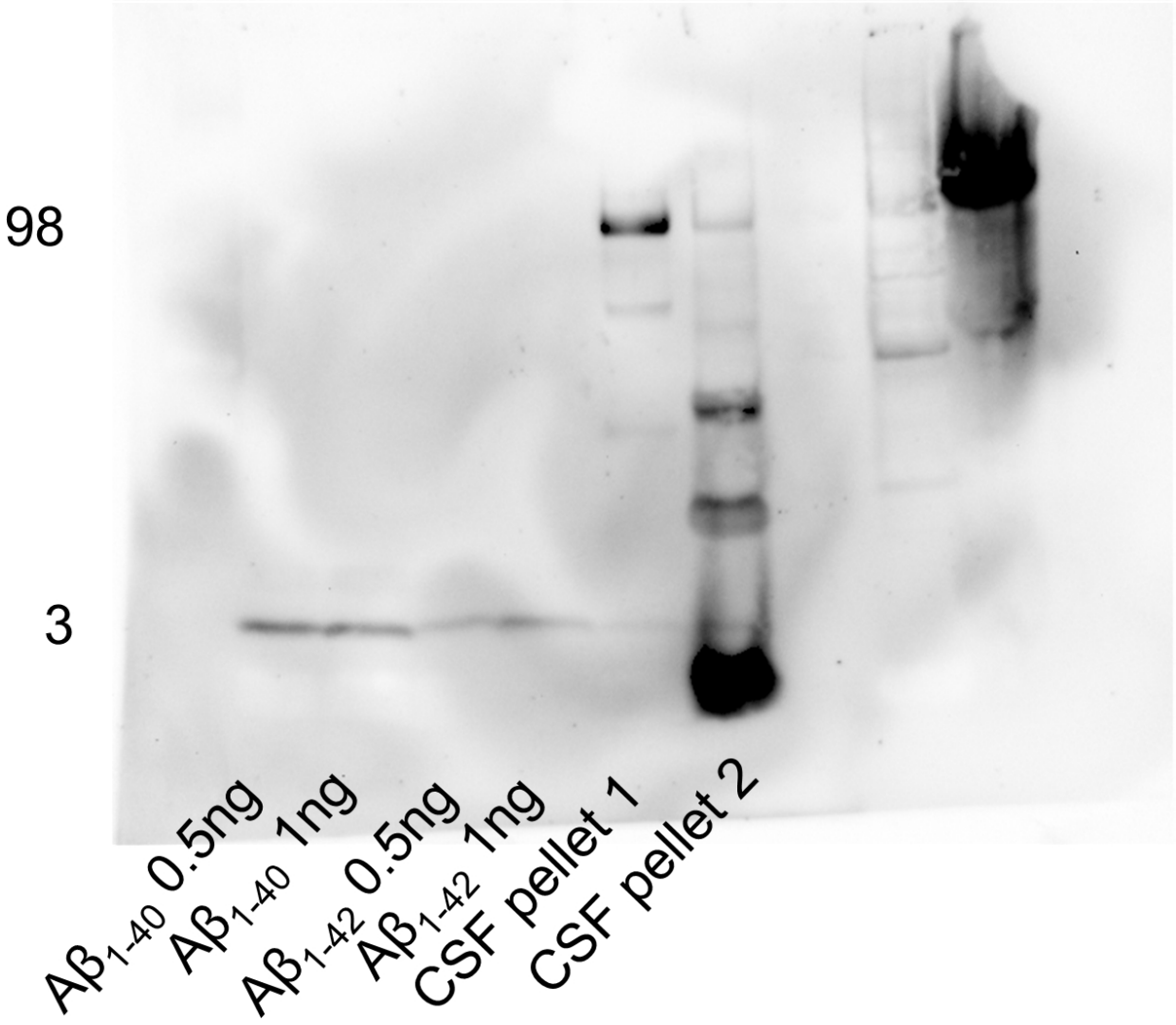

Uncropped scan 2 for Suppl. Fig. 16

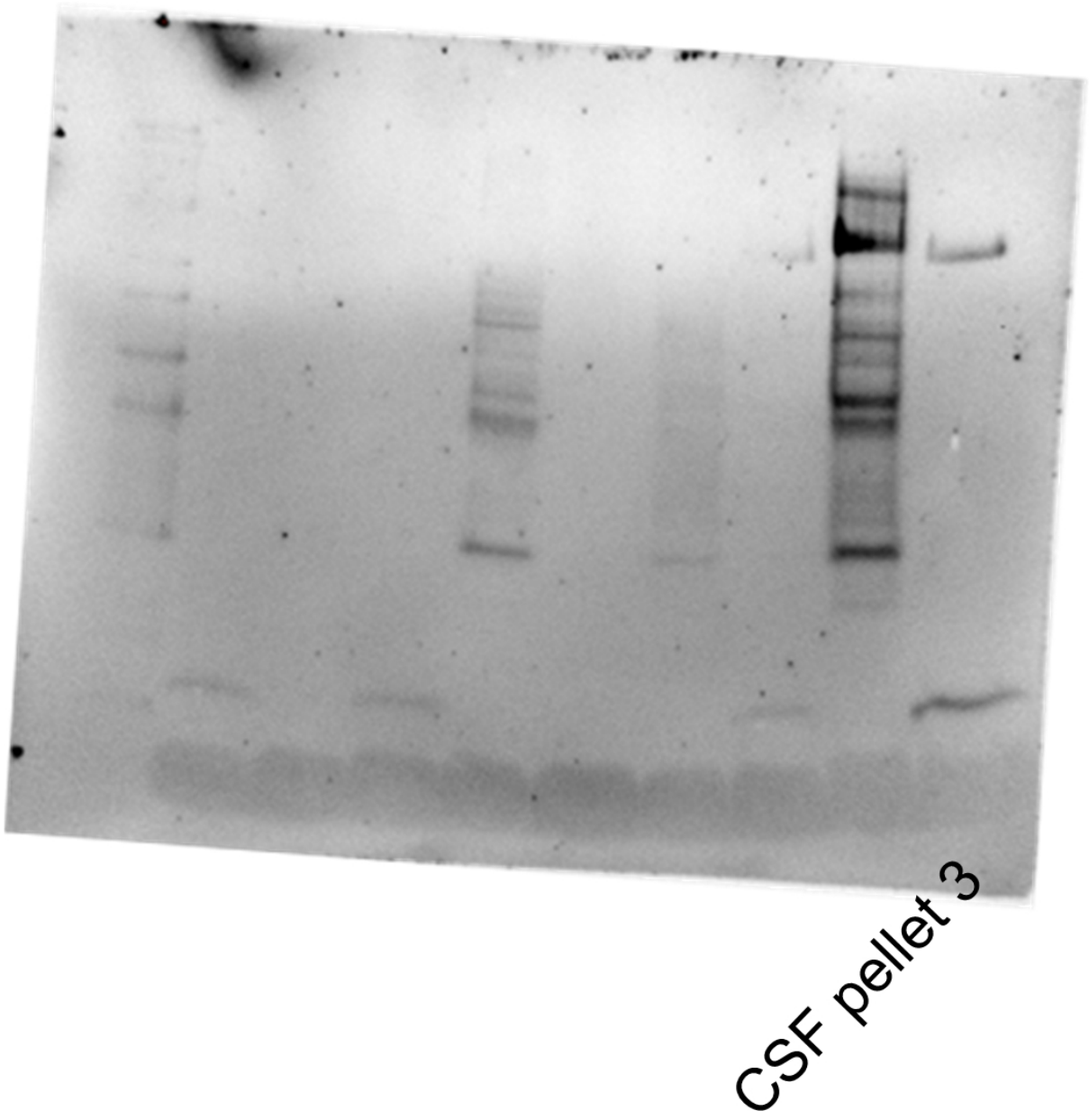

Part B. Supplementary tables

Suppl. Table 1.

Following intracerebroventricular injection, CFSE-labeled mononuclear cells or CX3CR1+ monocytes were tracked in the peripheral blood and lymph nodes of recipient mice two days later using flow cytometry. The numbers indicate the count of CFSE+ or CX3CR1+ cells, with the total events collected for each sample indicated in parentheses. High-intensity alignment green beads (6 µm) were injected into the lateral ventricle of three APP/PS1 mice as a control.

No.	Donor strain	Date of surgery	Animal ID	Sex	DOB	Age by cull (week)	LN	Blood
1	C57BL/6	19/02/2023	480	♀	11/11/2022	15	42 (666K)	1 (1.03M)
2	C57BL/6	19/02/2023	482	♀	11/11/2022	15	13 (40K)	3 (916K)
3	C57BL/6	05/02/2023	465	♂	10/10/2022	17		
4	C57BL/6	14/03/2023	475	♂	11/11/2022	18	1 (303K)	
5	C57BL/6	14/03/2023	479	♂	11/11/2022	18	1 (817K)	
6	C57BL/6	12/02/2023	472	♀	10/10/2022	18		
7	C57BL/6	12/02/2023	473	♀	10/10/2022	18	5 (869K)	
8	C57BL/6	26/03/2023	481	♀	11/11/2022	20	5 (131K)	10 (1.5M)
9	C57BL/6	05/02/2023	328	♂	11/07/2022	30		1 (1M)
10	C57BL/6	07/03/2023	92	♂	21/11/2021	68	31 (169K)	21 (663K)
11	C57BL/6	07/03/2023	80	♂	19/10/2021	72		4 (560K)
12	C57BL/6	04/06/2023	132	♀	12/01/2022	73		2 (573K)
13	C57BL/6	04/06/2023	96	♂	26/11/2021	80	2 (334K)	4 (845K)
14	Cx3CR1	23/09/2023	558	♂	18/01/2023	36	4 (76K)	1 (295K)
15	Cx3CR1	14/11/2023	559	♀	18/01/2023	43	5 (426K)	3 (2.4M)
16	Cx3CR1	16/09/2023	139	♂	23/03/2022	78	12 (212K)	4 (480K)
17	Cx3CR1	16/09/2023	140	♂	23/03/2022	78	7 (46K)	8 (1M)
18	Cx3CR1	23/09/2023	141	♂	23/03/2022	79	8 (242K)	5 (345K)
19	Beads	13/01/2024	620	♂	05/06/2023	32	0 (295K)	0 (1.5M)
20	Beads	13/01/2024	593	♂	08/02/2023	49	0 (379K)	0 (1.5M)
21	Beads	13/01/2024	520	♂	25/12/2022	55	0 (216K)	0 (1.5M)

Suppl. Table 2.

Comparison of surface Aβ levels and immune cell percentages among CU individuals with high brain Aβ-PET burden. CU individuals were categorized based on brain Aβ-PET status (CU-ve: ≤25 CL/CU+ve: >25 CL). Part 1 shows the results from the first round of flow cytometry examination of W0-2 and secondary antibody staining, including the percentage of Aβ++ monocytes and the mean fluorescent intensity of total monocytes in 141 participants (49 CU-ve, 29 CU+ve, 27 MCI+ve and 36 AD-dementia; 9 MCI-ve participants were excluded). Part 2 demonstrates the results from the second round of flow cytometry examination of W0-2 and secondary antibody staining, together with CD14, CD16, CD45 antibodies, including the percentages of NK cells and T&B cells, and monocyte subsets (intermediate, classic, and non-classic monocytes), the percentage of Aβ++ monocytes in the monocyte subsets, and the mean fluorescent intensity of the monocyte subsets in 108 participants (42 CU-ve, 22 CU+ve, 20 MCI+ve and 24 AD-dementia). Data is presented as Mean ± SD.

Part 1. Tube of W0-2+2nd	CU-ve (n=49)	CU+ve (n=29)	MCI+ve (n=27)	AD-dementia (n=36)
% of Aβ++ Monocytes	1.3±1	1.2±1.1	0.8±0.7	0.6±0.6
MFI of Monocytes	286±144.3	309.2±155.2	214.1±102.6	192.7±78

Part 2. Tube of W0-2+2nd and CD14, CD16, CD45	CU-ve (n=42)	CU+ve (n=22)	MCI+ve (n=20)	AD-dementia (n=24)
% of NK cells ($CD45^+CD14^-CD16^+$)	17±8	19.2±7.8	16.9±5.2	12.7±7.5
% of T&B cells ($CD45^+CD14^-CD16^-$)	83±8	80.8±7.8	83.1±5.2	87.3±7.5
% of Intermediate Monocytes	7±4.6	7.1±4.2	5.3±2.1	4.9±2.7
% of $Aβ^{++}$ Intermediate Monocytes	4±5.2	2.5±3.3	1.8±2.7	2.9±3.9
MFI of Intermediate Monocytes	475.1±471	356.4±299.2	293.7±271.7	416.4±352.3
% of Classic Monocytes	45±16.9	50.7±14.8	49.5±12.7	58.3±12.3
% of $Aβ^{++}$ Classic Monocytes	0.3±0.4	0.2±0.2	0.1±0.2	0.2±0.2
MFI of Classic Monocytes	161.1±93.6	168.7±111.1	129.8±73.4	138.2±59.4
% of Non-classic Monocytes	14.3±6.5	13.9±7.3	10.8±5.7	12.9±6.9
% of $Aβ^{++}$ Non-classic Monocytes	0.5±1.1	0.1±0.3	0.2±0.5	0.1±0.3
MFI of Non-classic Monocytes	114±119.9	87.1±43.4	92.4±72.3	101.5±62.2

Suppl. Table 3.

AUCs for different combinations.

Biomarkers (CL25)	Descriptives	Goodness of fit [a]	AUC (95% CI)	Brier improvement [b]
Baseline	Demographics (Age, Sex, Ed, APOE)	0.396	0.808 (CI: 0.721 to 0.895)	NA
BM1	MFI of Aβ on monocytes	0.424	0.827 (CI: 0.746 to 0.894)	3.3
BM2	MFI of Aβ on $Aβ^{+}$ monocytes	0.421	0.826 (CI: 0.762 to 0.901)	3.8
BM3	Percentage of $Aβ^{+}$ monocytes	0.415	0.828 (CI: 0.748 to 0.892)	3
BM4	Percentage of $Aβ^{++}$ monocytes	0.438	0.836 (CI: 0.761 to 0.899)	5.1
BM5	Percentage of $Aβ^{+}$ NK cells	0.477	0.848 (CI: 0.76 to 0.916)	7.1
BM6	Percentage of non-classic monocytes	0.396	0.818 (CI: 0.737 to 0.891)	-2.5
BM7	MFI of Aβ on $Aβ^{+}$ non-classic monocytes	0.39	0.816 (CI: 0.697 to 0.885)	-2.7
BM8	Percentage of $Aβ^{++}$ non-classic monocytes	0.418	0.824 (CI: 0.726 to 0.901)	0.7
BM9	Percentage of intermediate monocytes	0.418	0.83 (CI: 0.738 to 0.915)	0.3
BM10	MFI of Aβ on intermediate monocytes	0.413	0.828 (CI: 0.743 to 0.908)	0.2
BM11	Percentage of $Aβ^{+}$ intermediate monocytes	0.437	0.847 (CI: 0.764 to 0.921)	3.6
BM12	Percentage of $Aβ^{++}$ intermediate monocytes	0.423	0.834 (CI: 0.757 to 0.903)	1.2
BM13	Percentage of classic monocytes	0.441	0.844 (CI: 0.769 to 0.912)	3
BM14	MFI of Aβ on $Aβ^{+}$ classic monocytes	0.439	0.838 (CI: 0.75 to 0.908)	4
BM15	Percentage of $Aβ^{++}$ classical monocytes	0.45	0.838 (CI: 0.749 to 0.905)	4.8
BM16	MFI of Aβ on $CD45^{+}Aβ^{+}$ monocytes	0.457	0.844 (CI: 0.758 to 0.909)	5.4
BM17	Percentage of $CD45^{+}Aβ^{++}$ monocytes	0.446	0.834 (CI: 0.756 to 0.903)	1.7
New (Demo+BM4+ BM5+BM13+BM15)		0.528	0.871 (CI: 0.803 to 0.938)	13.5

We defined disease state simply by Centiloids >25CL for an "overall" assessment. [a]. A Hosmer–Lemeshow goodness of fit was used to test calibration of the model; [b]. The Brier score is the mean squared error of the model and the Brier improvement is the relative improvement of the brier score from the base model, which gives the percent improvement in accuracy with the addition of the biomarker.

Suppl. Table 4.

AUCs for single markers.

Biomarkers (CL25)	Descriptives	AUC
BM1	MFI of Aβ on monocytes	0.587
BM2	MFI of Aβ on $Aβ^{+}$ monocytes	0.568
BM3	Percentage of $Aβ^{+}$ monocytes	0.581
BM4	Percentage of $Aβ^{++}$ monocytes	0.639
BM5	Percentage of $Aβ^{+}$ NK cells	0.653
BM6	Percentage of non-classic monocytes	0.627
BM7	MFI of Aβ on $Aβ^{+}$ non-classic monocytes	0.599
BM8	Percentage of $Aβ^{++}$ non-classic monocytes	0.556
BM9	Percentage of intermediate monocytes	0.592
BM10	MFI of Aβ on intermediate monocytes	0.613
BM11	Percentage of $Aβ^{+}$ intermediate monocytes	0.668
BM12	Percentage of $Aβ^{++}$ intermediate monocytes	0.635
BM13	Percentage of classic monocytes	0.637
BM14	MFI of Aβ on $Aβ^{+}$ classic monocytes	0.654
BM15	Percentage of $Aβ^{++}$ classical monocytes	0.619
BM16	MFI of Aβ on $CD45^{+}Aβ^{+}$ monocytes	0.678
BM17	Percentage of $CD45^{+}Aβ^{++}$ monocytes	0.683

We defined disease state simply by Centiloids >25CL for an “overall” assessment.

Part C. Flow cytometry gating strategy

In the Methods section, we described “The flow cytometry-based assay”. The flow cyometry gating strategy can be found in Suppl. Fig. 3 (gating on forward scatter (FSC) and side scatter (SSC)),

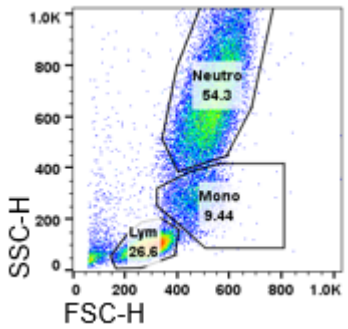

and Fig. 1 (gating on CD14 and CD16).

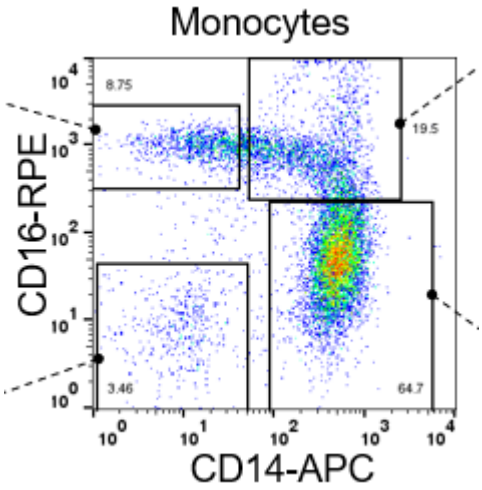

Monocytes are gated based on FSC/SSC in Fig. 4, and monocytic subsets are gated based on CD14 and CD16 in Suppl. Fig. 4.

The quantitative gating (Fig. 5, & Suppl. Fig. 7,8,9) can be found in the figures below:

For the single-color panel (1C) lymphocytes, L0-1.2 is W0-2 negative,

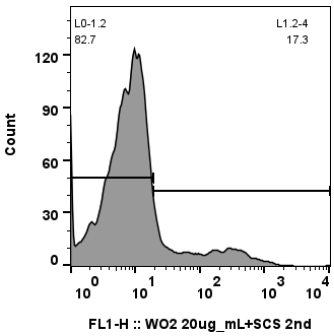

L1.2-4 is W0-2 positive.

For 1C monocytes, M0-2 is W0-2 negative, M2-4 is W0-2 positive, and M3.6-4 is W0-2 highly positive. The M3-4 is a test gating for W0-2 highly positive.

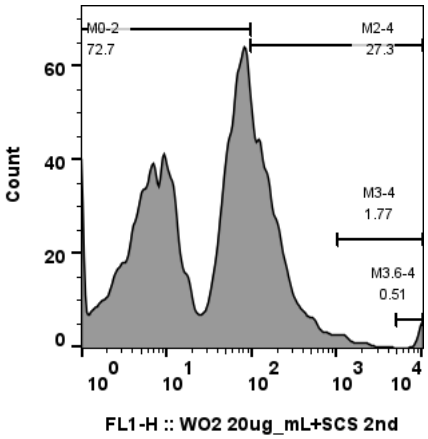

For the four-color panel (4C), CD45^{+} cells are gated first,

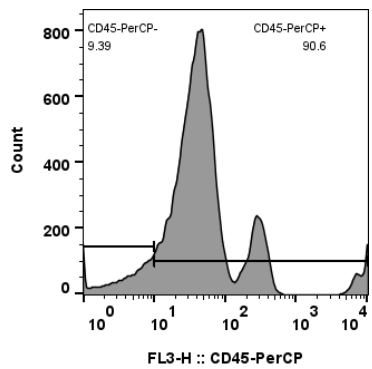

lymphocytes, and monocytes are then gated based on FSC/SSC,

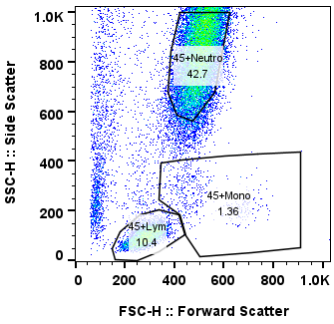

lymphocytes are then cleaned using $CD14^-$ gating and separated into NK cells and T&B cells using CD16 gating; monocytes are separated into non-classic, intermediate, and classic monocytes using CD14 and CD16 gating.

Fig. 6 illustrates the gating strategy for the CSF lymphocytes and monocytes.

Fig. 7 shows gating strategy for tracking injected monocytes in AD model mice.

Monocytes are gated based on FSC/SSC, and monocytic subsets are gated based on CD14 and CD16 in Suppl. Fig. 1.

Suppl. Fig. 5 depicts the gating strategy for the three-color real-time phagocytosis assay.

Cells are gated based on FSC/SSC, and are further gated by pHrodo-Abeta and AF647-Aducanumab in Suppl. Fig. 6a-b.

Monocytes are gated based on FSC/FSC, and further gated either based on pHrodo-Abeta/AF647-Aducanumab or CD14/CD16 in Suppl. Fig. 6c.

Cells are gated based on FSC/SSC, CD45, and CD14/CX3CR1 as shown in Suppl. Fig. 11.

In Suppl. Fig. 12, blood cells, deep lymph node cells, and brain cells are gated based on FSC/SSC, and further gated based on FL1-H and FL2-H. Beads are gated on FSC/SSC and are shown in FL1-H and FL2-H.

Part D. Antibody list for the study

22C11 (SigmaAldrich#MAB348)

4G8 made in house

6E10 made in house

AF488 goat anti-mouse IgG2a (Life Tech#A-21131)

AF647 CCR2 (BD# 558406)

AF647 CD163 (BD#562669)

AF647 CD35 (BD# 565329)

AF647 CD85A (BD#564469)

AF647 CD85D (BD#564345)

AF647 goat anti-mouse IgG2a (Life Tech#A-21241)

AF647 P2X7R (clone L4) made in house

CD11b-PE (BD#555388)

CD11c-APC (BD#559877)

CD14-APC (BD#340436)

CD16-PE (Dako#R7012)

CD33-PE (BD#347787)

CD45-PerCP (BD#347464)

CD4-PE (BD#555347)

CD68-FITC (BD#562117)

CD8-FITC (BD#555366)

CD91-PE (BD# 550497)

CX3CR1-PE (BD# 565796)

HLA-DR PE (BD#347367)

Lin1-FITC (BD#340546)

MerTK-APC (R&D#FAB8912A)

TREM2-APC(R&D#FAB17291A)

W0-2 made in house